ORIGINAL PAPER

Extensional neotectonics around the bend of the Western/Central Alps: an overview

Christian Sue · Bastien Delacou · Jean-Daniel Champagnac ·
Cécile Allanic · Pierre Tricart · Martin Burkhard

Abstract The Western Alps' active tectonics is characterized by ongoing widespread extension in the highest parts of the belt and transpressive/compressive tectonics along its borders. We examine these contrasting tectonic regimes using a multidisciplinary approach including seismotectonics, numerical modeling, GPS, morphotectonics, fieldwork, and brittle deformation analysis. Extension appears to be the dominant process in the present-day tectonic activity in the Western Alps, affecting its internal areas all along the arc. Shortening, in contrast, is limited to small areas located along at the outer borders of the chain. Strike-slip is observed throughout the Alpine realm and in the foreland. The stress-orientation pattern is radial for $\sigma 3$ in the inner, extensional zones, and for $\sigma 1$ in the outer, transcurrent/tranpressional ones. Extensional areas can be correlated with the parts of the belt with the thickest crust. Quantification of seismic strain in tectonically homogeneous areas shows that only 10–20% of the geodesy-documented deformation can be explained by the Alpine seismicity. We propose that, Alpine active tectonics are ruled by isostasy/buoyancy forces rather than the ongoing shortening along the Alpine Europe/Adria collision zone. This interpretation is corroborated by numerical modeling. The Neogene extensional structures in the Alps formed under increasingly brittle conditions. A synthesis of paleostress tensors for the internal parts of the West-Alpine Arc documents major orogen-parallel extension with a continuous change in $\sigma 3$ directions from ENE–WSW in the Simplon area, to N–S in the Vanoise area and to NNW–SSE in the Briançon area. Minor orogen-perpendicular extension increases from N to S. This second signal correlates with the present-day geodynamics as revealed by focal-plane mechanisms analysis. The orogen-parallel extension could be related to the opening of the Ligurian Sea during the Early-Middle Miocene and to compression/rotation of the Adriatic indenter inducing lateral extrusion.

Martin Burkhard deceased.

C. Sue · B. Delacou · J.-D. Champagnac · C. Allanic ·
M. Burkhard
Institut de géologie, Neuchâtel University,
Neuchatel, Switzerland

J.-D. Champagnac
CIRES, Boulder, CO, USA

P. Tricart
LGCA, UJF, Grenoble, France

C. Sue (✉)
UMR 6538, IUEM, place Copernic, 29280 Plouzane, France
e-mail: christian.sue@univ-brest.fr

Introduction and tectonic setting

The Alps include the relics of a major segment of the Tethyan Ocean and its continental margins (Fig. 1). According to the classical scenario (e.g., Coward and Dietrich 1989), rifting and subsequent spreading occurred in Mesozoic times between Europe and Adria, considered as an African promontory or an independent microplate (review in Wortmann et al. 2001). From the Late Cretaceous onwards, plate convergence resulted in the closure of the ocean and the thrusting of the southern margin onto the northern one (review in Schmid and Kissling 2000). In the discussion of the tectonics of the Western Alps, it is helpful to contrast the internal and external arcs.
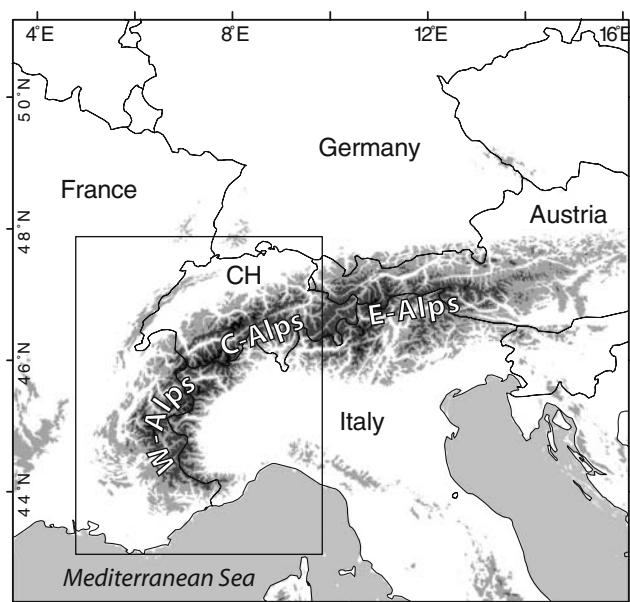
Fig. 1 Digital elevation model presenting the Alpine topographic configuration. The *inset* shows the studied zone in the Western and Central Alps. Note the prominent curvature of the belt toward its southern termination

The internal arc is mainly derived from an accretionary wedge assembled in Late Cretaceous to Eocene times, when the Tethyan Ocean and distal parts of the European margin were subducted below the Adriatic margin. Rocks of the internal arc display metamorphism generally increasing toward the East, reaching UHP conditions in places (review in Frey et al. 1999). The nappe pile of cover and basement rocks seen today is the result of a complex history of folding and thrusting during subsequent collision while the metamorphic conditions evolved from blueschist and eclogite to greenschist and amphibolite facies. The tectonic zone that best mirrors the arcuate shape of the Western Alps is the Briançonnais zone. It originally represented the NW-uplifted shoulder of the pre-oceanic rift and became later part of the European margin (Lemoine et al. 1986). In front of the Briançonnais zone, but limited to the northern part of the arc, the Valais zone bears witness to a narrow, short-lived ocean that probably merged with the Tethyan Ocean toward the East (Polino et al. 1990; Stampfli 1993). Southeast of the Briançonnais zone, the wide Piedmont zone originated from the distal European margin and from the Tethyan Ocean (Lemoine et al. 1986). Highly imbricated and folded cover nappes from both domains, built the Piedmontese Schistes lustrés complex. Dome-shaped inliers of continental basement nappes crop out in the Piedmont basement complexes of Monte-Rosa, Gran-Paradiso and Dora-Maira (internal crystalline massifs, ICM). Remnants of the overriding Adriatic margin are only preserved in the northern segment

of the arc (Dent Blanche klippe and Sesia zone, see Dal Piaz 1999 for a review).

The external arc (Dauphiné and Helvetic zones) is an NW- to SW-verging fold-and-thrust-belt derived from the proximal part of the European margin (review in Lickorish et al. 2002). Along the internal side of this arc, pre-Alpine European basement is massively involved in thrusting and folding. The high elevation of the external crystalline massifs (ECM) results from thrusting along deep-seated crustal-scale ramps from the Miocene onwards, and their uplift seems to have accelerated in recent times (review in Lacombe and Mouthereau 2002). The most external parts of the arc are the Subalpine Chains. Thrusting and folding in a thin-skinned fashion involved the Mesozoic cover, detached along Triassic evaporites. Deformation started in Oligocene times and moved progressively outward, the latest, most external thrusts override Serravallian molasse sediments, both to the NW (the Jura Arc overriding the Bresse-graben) and to the SW (Digne thrust overriding the Valensole basin).

The sharp present-day boundary between the external and internal arcs results from Oligocene first-order thrusting (Tricart 1984). A major thrust ramp, at the scale of the Alpine lithosphere, is best characterized along the ECORS-CROP deep seismic profile across the NE–SW segment of the arc (Nicolas et al. 1990). On geological maps, it mainly corresponds to the crustal Penninic front (CPF, front of the Valaisan or of the Subbriançonnais).

The Neogene to present evolution of the Western Alpine Arc is characterized by the change from collision to post-collisional extension (e.g., Sue and Tricart 2002, 2003; Champagnac et al. 2004, 2006; Selverstone 2005). In the Piedmont zone, ductile extension was replaced rapidly by brittle deformation, but in the Briançonnais zone it could have initiated directly in the brittle field. Extension in the internal arc was contemporaneous with folding and thrusting in the external arc. Decoupling between the internal and external arcs occurred along the CPF, where inversion of motion is observed in several places (e.g., Sue and Tricart 2002). Active tectonics is characterized by extension in the highest parts of the chain (Delacou et al. 2004). In this paper, we present an overview of these extensional processes.

Alpine neotectonics inferred from earthquake analysis and surface observations

In contrast to other Alpine orogenic belts, seismicity of the Alps is considered as low to moderate (Giardini et al. 1999). Nevertheless, historical catalogues (e.g., Fäh et al. 2003) show that the Western Alps and their foreland have undergone large earthquakes, with MSK intensity up to IX

and estimated magnitudes higher than 6 (e.g., 1356 Basel; 1855 St Niklaus; 1909 Lambesc). In the whole belt destructive earthquakes could potentially take place, particularly in the Valais in Switzerland, the Briançonnais and Provence in France, or Piedmont in Italy; however, some areas seem to be almost free of seismic activity (Ticino area, Switzerland; Vercors range, France). The first seismotectonic studies showed a radial fan for the *P*-axes around the Western Alpine Arc (Ahorner et al. 1972; Fréchet 1978; Pavoni 1980a, b; Ménard 1988).

By the end of the 1990s, an extensional regime was recognized in the internal zones of the belt, but locally also in some areas situated in the external zones (Maurer et al. 1997; Eva et al. 1998; Sue et al. 1999; Baroux et al. 2001; Kastrup et al. 2004) (Fig. 2). At first, extension was considered a local phenomenon, resulting from secondary tectonic complexities within a collisional system; however, with increasing data density extension became a first-order characteristic of Alpine neotectonics (Sue et al. 1999; Sue and Tricart 2003; Delacou et al. 2004). Indeed, the Western Alps reflect two contrasting tectonic regimes, with a more or less important extension in the core of the belt and localized compression in outer areas. Strike-slip movements also occur everywhere in the belt.
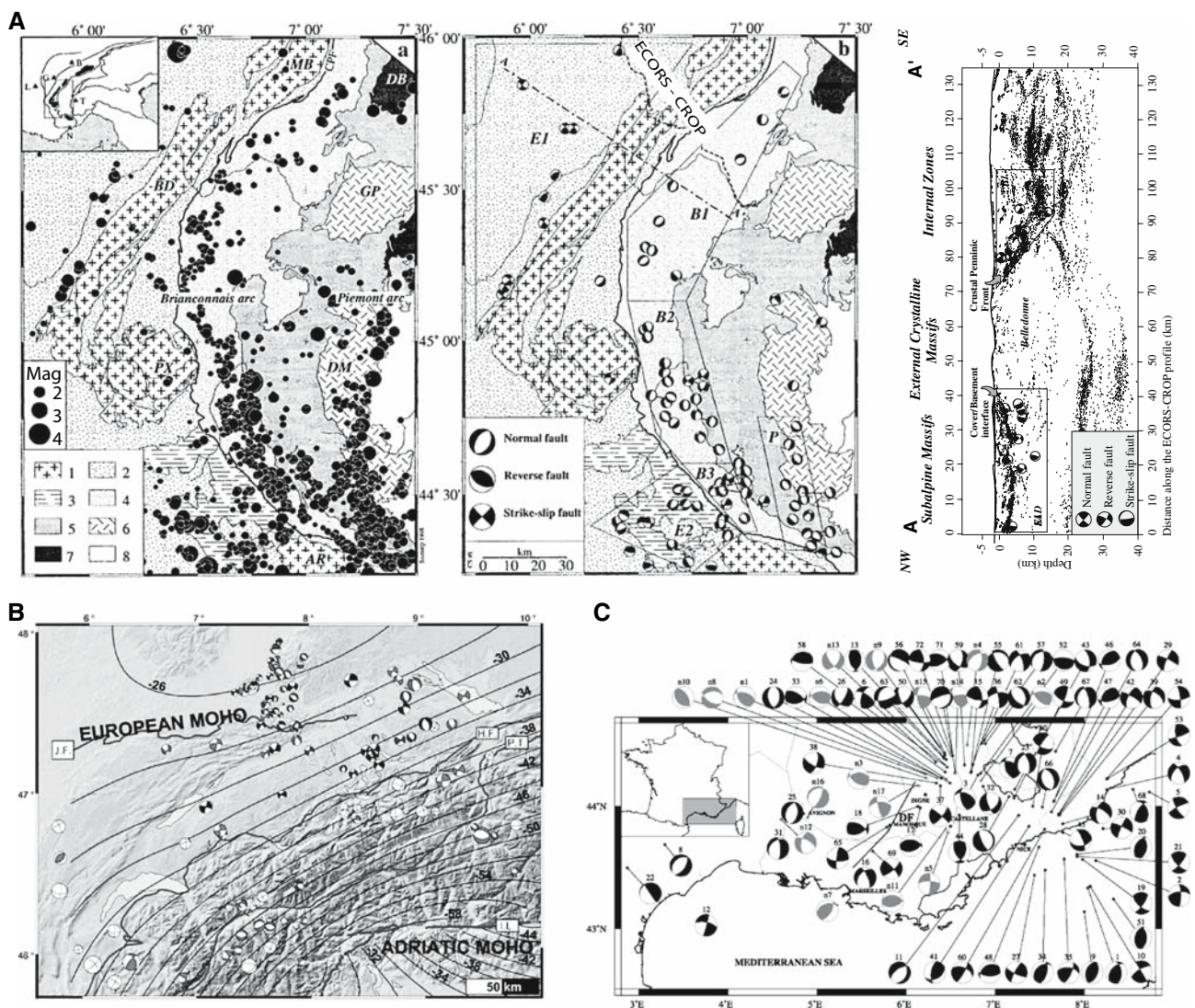

Fig. 2 Regional seismotectonic data from the arc of the Western and Central Alps documenting extensional tectonics **a** Western Alps after Sue et al. (1999) (boxes: *1* represents external crystalline massifs EMC, *2* represents Meso-Cenozoic sedimentary cover of ECM, *3* represents Flysch décollement nappes, *4* represents Briançonnais zone, *5* represents Piedmont zone, *6* represents internal crystalline massifs, *7* Ophiolites, *8* Austro-Alpine units; the crustal Penninic front is represented by the *bold line*. Massifs: *PX* Pelvoux, *MB* Mont-Blanc, *BD* Belledonne, *AR* Argentera; *DB* Dent Blanche, *GP* Gran Paradiso, *DM* Dora Maira. Towns: *B* Bern, *G* Genève, *L* Lyon, *N* Nice; *T* Torino.); **b** Switzerland, after Kastrup et al. (2004). Depth of Moho in kilometers; **c** Provence area, after Baroux et al. (2001). See text for details

In this part, we will analyze the relationships between Alpine structures, faulting, and seismicity and then we will focus on a synthesis of modern seismotectonic data. We used previous studies (Ménard 1988; Eva and Solarino 1998; Sue et al. 1999; Baroux et al. 2001; Kastrup et al. 2004) to build a database including 389 reliable focal mechanisms, which has been extensively described by Delacou et al. (2004).

Alpine structures, faults, and seismicity

Here we identify potentially active faults recognized at the surface in order to establish the relationships between large-scale inherited crustal structures and seismicity.

The seismicity localized to the SE of the Pelvoux massif, along the southern part of the so-called Briançonnais seismic arc, is limited to the upper crust with hypocenters not deeper than some 15 km (Rothé 1941; Sue et al. 1999; Sue and Tricart 2003) (Fig. 3). The earthquakes are concentrated along and immediately to the east of the CPF, except below the Embrunais-Ubaye flysch nappe in the saddle between the two basement culminations of the Pelvoux and Argentera massifs (Ménard 1979). In the Briançonnais zone, just east of the CPF, seismicity occurs in NNW–SSE elongated clusters, following the arcuate shape of the CPF. This seismic activity correlates with the fault network mapped at the surface, and particularly with a family of longitudinal faults described by Sue and Tricart (2003). Three major faults observed in the field seem to be seismically active: the high-durance fault (HDF), the Serennes-Bersézio fault (SBF), and the East-Briançonnais fault (EBF) (Fig. 3). The depth of the hypocenters and the geometry of the CPF and thus the 3D-geometry of the Briançonnais zone, suggest that the seismicity along these three active faults is restricted to the Briançonnais units; in others words, seismicity remains located above the CPF as already shown to the North along the ECORS profile (see cross-section Fig. 2 a, and Sue et al. 1999; Sue and Tricart 2003). Focal mechanisms indicate mainly normal faulting, with focal planes compatible with the directions of the seismic alignments. A few strike-slip mechanisms follow the longitudinal fault system with right-lateral motion, but they could also be related to left-lateral motion along transverse faults. Indeed, observations in the field confirm these senses of motion. Figure 3 illustrates the geometry and the kinematics of three active faults recognized in the field.

The high-durance fault

The seismic activity along the HDF corresponds to the western earthquake clusters on the six cross-sections of Fig. 3 a. This active fault branches on the CPF at depth

(Sue and Tricart 1999, 2003). This characteristic is also recognized on a larger scale along the ECORS profile, to the North of the Briançonnais seismic arc (Fig. 2 a). A zoom on the Briançon region (Fig. 3 c) confirms that the orientations of the seismic clusters correspond to faults belonging to the HDF system mapped at the surface. Focal mechanisms indicate normal faulting in agreement with mapped structures showing down throw to the East (Sue and Tricart 2003).

The East-Briançonnais fault

The eastern clusters of cross-sections A2/B2, A3/B3, and A7/B7 (Fig. 3 a) correspond to the EBF. The focal mechanisms indicate normal faulting with some strike-slip component compatible with dextral motion along the EBF. On Fig. 3 c, we see that the seismic clusters are well correlated with the outcrops of the fault. This normal fault roots deeper than the HDF and SBF, possibly because of a more important transcurrent component.

The Serennes-Bersézio fault

Cross-sections A5/B5, A8/B8 (Fig. 3 a), and zoom Fig. 3d illustrate the SBF. It seems to affect a deeper part of the crust than the HDF. The distribution of hypocenters corresponds to the surface fault system oriented N130°. This fault works as a normal fault with a dextral component, as shown by structural data (Sue and Tricart 2003). The relationships between the SBF and the CPF appear, however, to be more complicated. The SBF is closer to the CPF than the HDF, and it seems that it merges with the CPF at depth. We may propose two interpretations: either the seismicity of the SBF merges and follows the CPF at depth, or the SBF cuts the CPF and offsets this former thrust (Fig. 3d). The first hypothesis would imply a direct reactivation of the CPF as a normal fault, and a quite steep geometry for the original thrust.

The Font-Sancte area, in the Queyras and High-Ubaye massifs (location on Fig. 3d) shows a well-developed fault system linked to the SBF, which controls the local and overprints the glacier-related morphology. A family of transverse faults (N50°–N80°) shows a horsetail termination, just east of the Serennes longitudinal fault (N150°, segment of the SBF, Fig. 4). The main transverse fault runs through the Font-Sancte peak (Fig. 4c, d), from where it can be traced for about 15 km to the East. Other minor transverse faults develop in a fan-shape pattern South of the Font-Sancte fault, reactivating also a Jurassic extensional fault (Claudel et al. 1997). Kinematic analysis of this fault system shows that the Serennes fault behaves mainly as a dextral and the transverse faults behave as sinistral strike-slips. The asymmetric fan-structure of the transverse
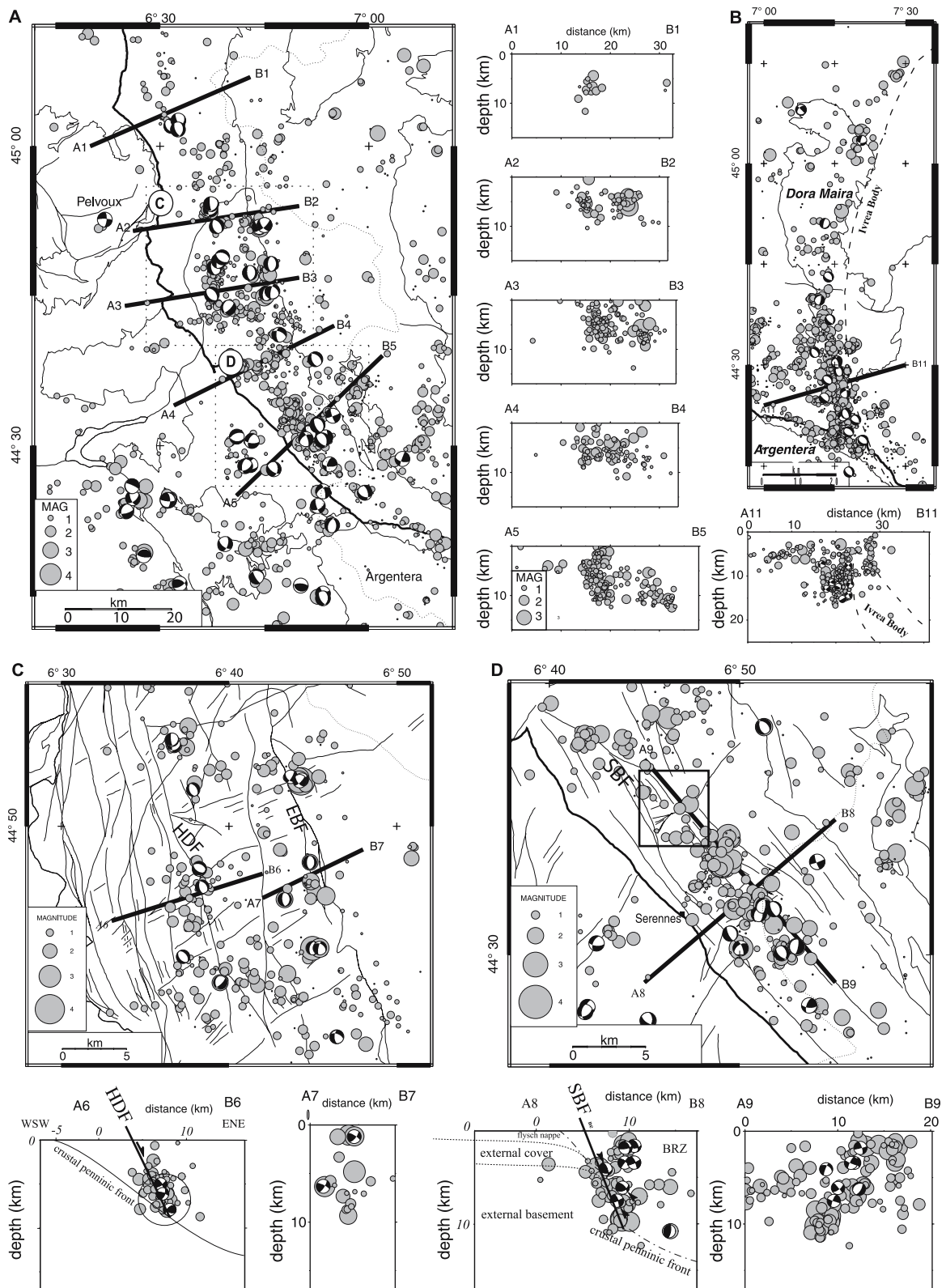
Fig. 3 Seismotectonic maps and cross-sections in the Southwestern Alps, across the Briançonnais and Piedmont seismic arcs (see Fig. 2a for location). The relationships between inherited crustal structures (rustal Penninic ront and Ivrea Body) and seismicity (Briançonnais and Piedmont arcs) are illustrated in **a** and **b** (respectively). Zooms on the Briançon (**c**) and Ubaye (**d**) areas allow to localize the seismic activity along faults recognized in the field: High-durance fault, Serennes-Bersézio fault, and East-Briançonnais fault. *Square* on map (**d**) indicates the Font-Sante area (Fig. 4). See text for details
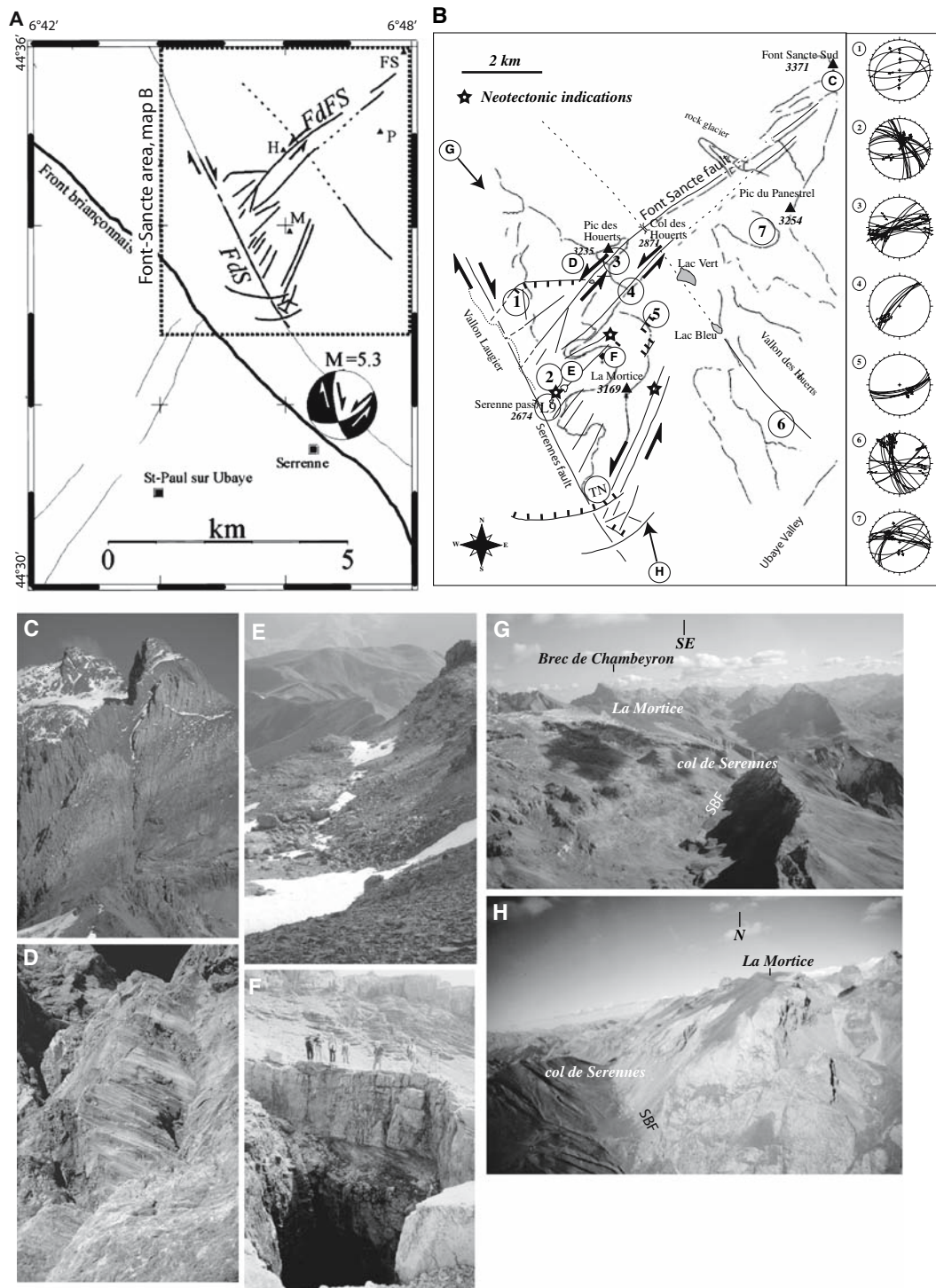
Fig. 4 Examples of fault-controlled morphology: the Font-Sancte area (Southwestern Alps, see Fig. 3 for location). **a** Location of the major Serennes earthquake (1959, Ml = 5.3, after Ménard 1988). Note the correlation between focal mechanism and tectonic characteristics inferred from structural data in terms of fault orientation and fault kinematics. *FdFS* Sinistral Font-Sancte fault, *FdS* Dextral Serennes faults. **b** Tectonic sketch map of the area, showing the location of the structures illustrated in **c** to **h**. *Numbers 1–7* indicate the location of the fault/striae measurements plotted to the right. Note the extensional components of motion. *Stars* indicate neotectonic

structures such as reverse slopes in moraines (example in **e**). **c** Eastward view of the Font-Sancte left-lateral fault. **d** Large striated plane (30 m high) along the Font-Sancte fault at the Col des Houerts pass. **e** Reverse slope in scree and moraine along the transverse fault system. **f** View of the Mortice cave developed along transverse faults that define the walls of the cave. **g** and **h** southeastward (**g**) and northward (**h**) aerial views of the Serennes fault showing the relationships between the main Serennes longitudinal fault and the transverse fault system (Font-Sancte fault type)

system reflects this tectonic configuration, the two directions working contemporaneously. Normal faulting has also been observed along these structures.

This area presents several neotectonic structures such as several-hundred-meters-long counter slopes in talus-scree and moraines (example Fig. 4e, stars in Fig. 4b). Moreover, the small river in the Serennes Valley presents three topographic anomalies that could be due to recent left-lateral offsets along transverse faults (Fig. 4b). A karst system also developed along the transverse fault system (e.g., a vertical cave 110 m deep, Fig. 4f). The Terres Noires fault, to the South of this area is characterized by a fault scarp of several metres. It could be interpreted as an active fault or as an inherited structure, because it is located on the hinge of an anticline. However, this area is very close to the epicenter of the so-called Serennes earthquake (1959, Ml = 5.3, MSK intensity VII–VIII, Ménard 1988). The earthquake occurred at about 2–3 km to the South of the Font-Sancte area, but the potential error in its location is about several km (Fig. 4a). The focal mechanism proposed by Ménard (1988) is coherent with our neotectonic analysis (right-lateral slip on a plane parallel to the Serennes fault or left-lateral slip on a plane parallel to the transverse faults). Thus, taking into account the location error, we may speculate that this quake activated one of the faults in the Font-Sancte area. Local observations show that part of the regional brittle deformation took place in Pliocene to recent times, accompanied by seismic activity.

The crustal Penninic front

In map view (Figs. 2 a, 3 a) the Briançonnais seismic arc follows the CPF, reflecting a control of this older, Oligocene, thrust on the seismicity (Sue et al. 1999, 2002). As shown above, active faults (HDF and SBF) branch on the CPF at depth. By projecting the focal mechanisms of the northern part of the Briançonnais seismic arc onto the ECORS profile (Fig. 2 a) we may see that extensional focal mechanisms are associated with the reflector imaging the CPF, suggesting a young extensional reactivation of this crustal structure. The CPF thus appears as a major discontinuity inherited from the compressional Alpine history that controls and localizes the active extensional deformation, seismically expressed along the Briançonnais seismic arc. Nevertheless, extensional movements are not limited to the CPF, but also affect more external areas (Delacou et al. 2004).

The Ivrea Body

The Piedmont seismic arc (Fig. 2a) is completely separated from all surface structures of the Western Alps, crossing

geological boundaries at the southern tip of the belt; however, seismicity nicely correlates with the gravimetric and seismic-velocities anomalies associated with the Ivrea Body (Fig. 3b) (e.g., Bayer et al. 1989; Paul et al. 2001; Sue et al. 2002). This striking spatial correlation suggests a causal relationship between seismic activity and the presence of the Ivrea mantle rocks imbricated with the middle to upper crust. Indeed, the Piedmont seismic arc follows rather perfectly the –25 mGal contour and the western side of the Ivrea Body (Sue et al. 2002). In contrast to the arcuate surface structures of the southernmost Western Alps, the geometry of the Ivrea Body is quite linear. Focal mechanisms exhibit mostly normal faulting, albeit with some uncertainties arising from high-velocity contrasts. The present-day tectonics of this area is not as clear as for the Briançonnais seismic arc, and some mix between normal faulting, strike-slip and may be even thrusting could occur in this sector. Nevertheless, despite these shortcomings, extensional movements seem to prevail, just as in the rest of the internal zone of the belt (Fig. 3b).

Comparative analysis

The Briançonnais and Piedmont seismic arcs are both linked to mechanical discontinuities and crustal structures inherited from a long and complex Alpine tectonic history (CPF and Ivrea Body). Both seismic arcs currently display a similar tectonic behavior with a predominance of extension. In detail, however, there are subtle differences. The Piedmont seismic arc seems to affect a slightly deeper portion of the crust, with a maximum of activity in the 10–15 km range, the seismically active zone cutting across surface structures with a rectilinear shape. The Briançonnais seismic arc, on the other hand, is concentrated within the topmost 10 km of the crust and follows the arcuate geometry of the belt. In order to compare the mechanical behavior of these two seismic arcs, a statistical analysis has been conducted based on the energy and space distributions (Sue et al. 2002). Space distributions (D-value) of both seismic arcs show similar values of 1.9 and 2.0; both present typical energetic power-law distributions, with a classical b-value of 1 for the Briançonnais arc and a significantly lower b-value of 0.7 for the Piedmont arc. After comparison with mechanical models (Amitrano et al. 1999), these variations of energetic distributions have been interpreted in terms of ductility versus brittleness. The Briançonnais seismic arc would present a globally more brittle behavior compared to the more ductile Piedmont seismic arc. These differences could stem either from the depth distribution of seismicity, a different mode of deformation depending on rock composition (upper crustal rocks versus mantle indenter), or weakened rocks inherited from older structures.

Neotectonic synthesis

In a neotectonic low-strain area such as the Western Alps, it is quite difficult to observe clear indications of neotectonic activity because of the high erosion rates and recent glaciation. Nevertheless, three types of observations can be used to detect active faults in the Alps: the relative location of hypocenters, their alignments that follow mapped faults, and geomorphic indicators.

The relative relocation of earthquakes is a powerful method applied to seismic sequence in order to determine the geometry of active faults. It is based on cross-correlation (time or frequency) of similar seismograms (similar body waves due to similar ray-paths). This method gives the relative location of the event of a given crisis with respect to the master event, with an overall precision in the order of tens of metres (e.g., Fréchet 1985; Deichmann and Garcia-Fernandez 1992; Maurer and Deichmann 1995). In most Alpine cases, the alignment obtained using relative relocations is coherent with one of the nodal planes of the main shock's focal mechanism. These types of relocations

in the Western Alps have been compiled on the map Fig. 5 a (red symbols) after Deichmann and Garcia-Fernandez (1992), Augliera et al. (1995), Maurer and Deichmann (1995), Kastrup et al. (2004), and Delacou et al. (2005b).

The precise analysis of seismic alignments is used in the case of rather diffuse seismic activity in a relatively small area. This method is less accurate than the relative relocation, as it only allows defining seismic alignments and fault zones rather than an active fault plane. The Wildhorn fault zone of the North-Valais area (Switzerland) is a good example of such an alignment (Maurer and Deichmann 1995). This seismic zone represents a subvertical right-lateral fault system at least 60 km long, running in a WSW–ENE direction, sub-parallel to but some 10 km to the north of the Rhône Valley. Relative relocation studies of given seismic crises have shown that individual faults are oblique with respect to the overall direction of the seismic alignment. These faults could be interpreted as secondary Riedel shears, distributed along an en-échelon system related to a master fault. A synthesis of the seismic alignments observed in the Western Alps is also presented
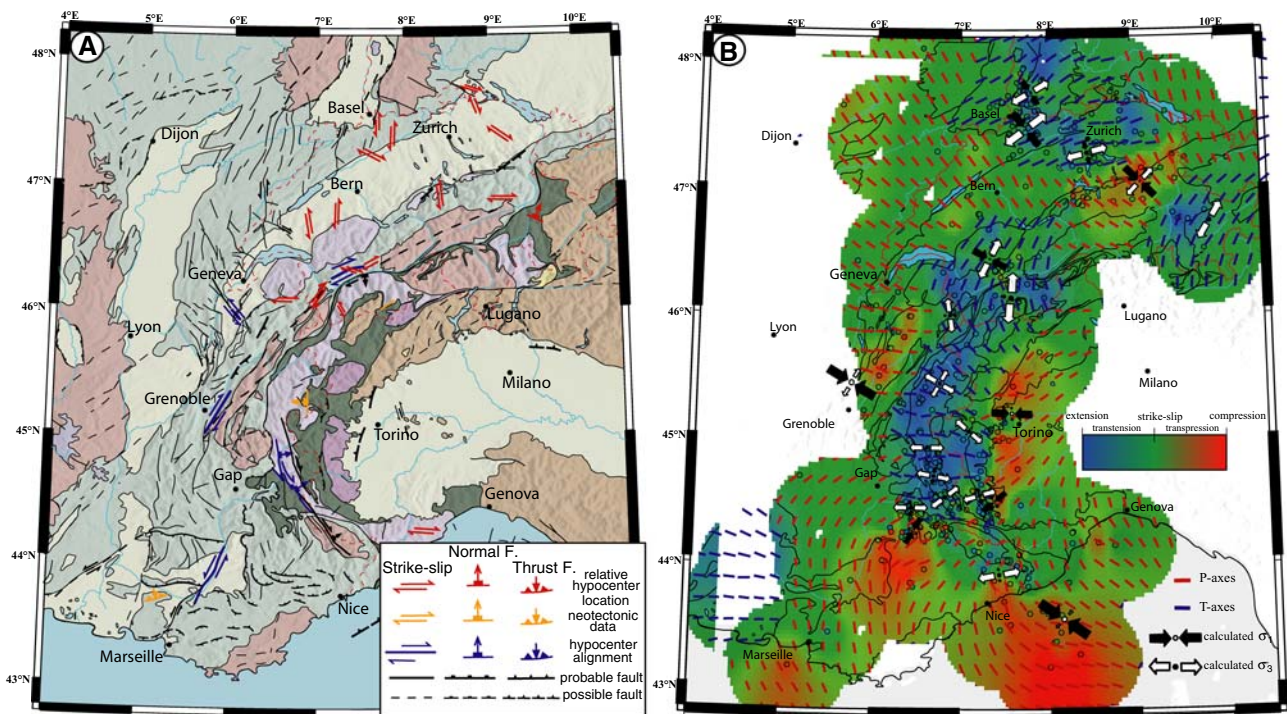

Fig. 5 a Neotectonic map of the Western and Central Alps. The classification in the inset provides a measure of the reliability of mapped faults and fault systems, with a reliability decreasing from faults identified by seismic relative location techniques (in *red*), neotectonic field observations (in *orange*), seismic alignments (in *blue*) to probable and possible ones (in *black* and *dotted black*). Note the occurrence of a widespread dextral fault system following the western side of the belt from the northern Valais to the front of Belledonne and the Briançonnais/Argentera areas (Fig. 2). See text for details. **b** Regionalization of deformation and stress inversion

computed from the seismotectonic database of Delacou et al. (2004). *Blue* represents extension, *green* represents strike-slip, and *red* represents compression, interpolated from the dip of the *P* and *T*-axes. *Red* and *blue bars* represent interpolation of *P* and *T*-axes orientations. *Black* and *white arrows* represent σ1 and σ3 directions calculated by stress inversion. Note the correlation of extensional areas in the core of the belt with orogen-perpendicular extension. The external domains are characterized by a transcurrent system with localized changes toward compression or extension, and by orogen-perpendicular fan-shaped directions of compression

on Fig. 5 a with blue symbols (Eva et al. 1998; Thouvenot et al. 1998; Thouvenot et al. 2003).

Very few and isolated field studies in the Western Alps have allowed to identify active faults (orange symbols on Fig. 5 a compiled after Lacassin et al. 2001, and Champagnac et al. 2006). Displaced Quaternary deposits provide circumstantial evidence for post-Würm offsets which have been correlated with regional seismicity in order to evaluate the coherency of the neotectonic indications. In all cases, it remains difficult to discriminate between active faulting and non-seismic deformation (landslides, etc.). In a few isolated cases, however, indications such as the continuity of a given structural alignment, the compatibility with the stress/strain fields, and occurrence of colluvial wedges , allow to propose a tectonic origin for Quaternary structures.

In our map (Fig. 5 a), these seismotectonic and neotectonic data have been complemented by faults recognized in the field but not proved to be active. The latter are qualified as ''probable faults'' (continuous symbols) if they are well integrated in the regional stress/strain fields, and ''possible faults'' if they occur in an area of ill-defined seismotectonic regime. Our neotectonic map also includes the stress axes computed from the inversion of focal mechanisms (see hereafter).

Current strain and stress fields inferred from seismotectonics

In this part, we will analyze the Alpine seismicity from a general viewpoint, on the basis of a large-scale focal mechanism synthesis built by Delacou et al. (2004). Figure 2 groups the main maps used in this compilation. The aim of this part is no longer to identify active structures, but to characterize the current stress-and-strain fields around the bend of the Western and Central Alps. Our database contains 389 reliable and carefully checked focal mechanisms. The local magnitudes (Ml) are in the (0.7–6.0) range for events recorded between 1969 and 2000.

Regionalization of the deformation

We used our database primarily to constrain the current state of deformation in the belt and to map the stress field. A scalar parameter has been assigned to each focal mechanism following the dip of the P and T-axes (see Delacou et al. 2004 for details, Sect. ''Discussion'', and critical review of the method). This scalar parameter was then interpolated, in order to draw a map of the state of deformation covering the entire Western and Central Alps (Fig. 5b). Despite the limitations and artefacts of this approach, this large-scale regionalization allows the recognition of homogeneous zones in terms of deformation state.

The most important characteristic is a continuous zone of extension in the internal zones of the chain, all along the belt from the Southern Valais to the north of the Argentera massif (Fig. 5b). This zone of extension might well extend even further to the east into the Grisons area, but its continuity in the western areas is not documented across the Lepontine dome, which lacks seismicity. The second main characteristic is the existence of small discontinuous areas with a compressive/transpressive regime localized along the outer borders of the Alpine chain. Compression occurs in the Eastern Helvetic domain, in front of the Belledonne massif, in front of the Digne nappe and in the Western Po plain. In terms of trajectory fields of P and T-axes, our map confirms the radial fan-shaped distribution of T-axes in the internal zones (orogen-perpendicular extension), and of P-axes in the outermost zones (Fréchet 1978; Pavoni 1980b; Ménard 1988).

Stress inversion

The second level of analysis performed on the basis of our focal mechanism synthesis was the inversion of the current stress field (Delacou et al. 2004). Here, we summarize some of the main characteristics of this stress field, which then will be interpreted in terms of Alpine dynamics. For the discussion of the various inversion methods we refer to Delacou et al. (2004). Delacou's inversion is based on a selection of homogeneous zones, characterized by a uniform type of deformation in terms of regionalization, and integrating the information obtained from the P/T-axes orientations. The resulting stress field is shown in Fig. 5b. Our results are consistent with previous regional studies (e.g., Maurer et al. 1997; Sue et al. 1999; Baroux et al. 2001; Kastrup et al. 2004).

In the internal zones, an orogen-perpendicular extensional stress field is continuous all along the inner arc of the belt. It is systematically found at a high angle to the CPF. The $\sigma 3$ direction changes from almost N–S in the South Valais, to E–W in the Central Briançonnais area, and NE–SW in the southern part of the Briançonnais. This radial extension characterizes also the Piedmont seismic arc. The external zones are characterized by contrasting states of stress, with the three possible tectonic modes: strike-slip, extension, and compression. Strike-slip dominates the lateral variations of the tectonic mode toward extension (transtension) or compression (transpression). Principal stress directions are coherent along the external zones, rotating progressively and defining a radial fan pattern of $\sigma 1$, which is perpendicular to the belt, from a NNW–SSE direction in Northern Switzerland to NW–SE in front of Belledonne and SW–NE in front of the Digne nappe. In the foreland of the Alps, the Rhine graben system is in a state of transtensive stress that continuously extends southeast-

wards into the Eastern Jura. The Ligurian margin presents a compressive stress state, with $\sigma 1$ oriented NW–SE perpendicular to the extensional structures of the Oligocene Ligurian opening (Béthoux et al. 1992). To sum up, the current stress field around the bend of the Western and Central Alps is characterized by a generalized and continuous orogen-perpendicular extension in the core of the belt, contrasting with localized zones of transpression at its outer limits.

GPS data and seismotectonics

The determination of GPS-related strain rates based on a synthetic database, harmonized by Nocquet and Calais (2003), takes into account measurements from permanent stations (ITRF2000, RGP, REGAL, EUREF-EPN) and temporary stations (RRF 1993–1996, Jura 2000, Rhin 1999–2000, Alpes 1993–1998). It clearly shows a good agreement with the overall seismotectonic regionalization described earlier. Extension characterizing the high chain is welldocumented in GPS strain maps, with almost the same geographical distribution (where the density of GPS data is sufficient) and the same directions of extension. Moreover, in the external domains, seismotectonically compressive areas along the northern front of the Belledonne massif, the Provence area and the border of the Po plain are also well imaged by GPS data. Our study therefore strengthens the qualitative analysis of seismotectonic deformation and provides further quantitative information about strain rates. For extensional areas, maximum values of stretching reach $3–6 \times 10^{-08}$/year, whereas for compressional areas, maximum values of contraction reach $–4$ to $–6 \times 10^{-08}$/year. These maxima, corresponding to strain rates of about 1–3 mm/year with respect to a 50-km baseline, are compatible with local previous studies (Martinod et al. 1996; Sue et al. 2000; Martinod et al. 2001) that yielded strain rates of about 2 mm/year for E–W oriented extension in the Briançonnais area (Sue et al. 2000), and 3–5 mm/year for compression/strike-slip deformation in the front of the Belledonne massif (Martinod et al. 1996, 2001). At a larger scale, 0.5 mm/year of extension have been observed between Lyon and Torino (Calais et al. 2002; Nocquet and Calais 2003). Seismic strain quantification shows a good qualitative coherency between the strain field as measured by GPS in terms of the mode and direction of deformation. In terms of absolute values, a maximum of 10–20% of the deformations measured by GPS can be explained by the current seismicity (Sue et al. 2007). This important discrepancy between seismic strain and geodetic strain remains to be explained. The following are the possible reasons : an important contribution of

aseismic deformation within the Alps, interpreted in terms of elastic loading, creeping, and/or ductile deformation (Fig. 6).

Relationship between crustal thickness and mode of deformation

We used a digital elevation model (DEM; smoothed with a 50-km bin) as a proxy for the topographic load of the Alps. This smoothed topography shows a very good correlation with crustal thickness and documents the large-scale relationship between average topography and deformation mode (Fig. 7). Maxima in average topography exist in Eastern Switzerland, in the Valais and in the Vanoise areas, whereas more localized and isolated high mountains in the external zones, such as the Mont-Blanc massif, almost disappear in the 50-km bin smoothing. Except for the Ivrea Body, negative Bouguer anomalies in the Alps (Masson et al. 1999) are closely correlated with zones of increased crustal thickness reflected by the Moho depth contours (Waldhauser et al. 1998) (Fig. 7). In order to visualize the relationship between deformation and topography, the map of the regionalized deformation was draped over the smoothed Alpine topography. In this 3D-image, the high chain (the convex crestline of the Alps) appears to match very closely the areas undergoing extension (Delacou et al. 2004). Moreover, transpression nicely coincides with the negative (concave) curvature at the transition between the Alps and their foreland. In summary, a close correlation exists between extensional tectonics and the zones of increased crustal thicknesses, the so-called ''high chain''.

Numerical modeling

The close correlation between areas of increased crustal thickness and the generalized extensional tectonics leads to propose a geodynamic model where the current Alpine tectonic regime is to a large part controlled by gravitational body forces. Gravitational potential anomalies (GPA) driven by lateral variations in crustal thickness between internal and external zones could induce extension in high internal zones. In response to this extension, external areas would undergo compression in an attempt to equilibrate crustal thicknesses. Such a tectonic model could well explain the radial extensional stress axes in high-elevation areas in the core of the belt as well as the radial compressive stress axes in low-elevation areas along its borders. In the following, we test this intuitive interpretation using two different approaches.

Fig. 6 Geodetic versus seismic strain quantification. In order to be interpretable, quantifications are converted into mm/y considering typical baselines of 50 km. The background colors represent geodetic estimates of strain rates with the same color code as in Fig. 4 (*blue* represents extension, *red* represents compression); the *small blue and red bars* show the calculated directions of extension and compression, respectively. *Large bars* represent estimates of strain rates (based on seismic data of Fig. 4). Their length gives magnitudes of strain rate (*scale in top left*)
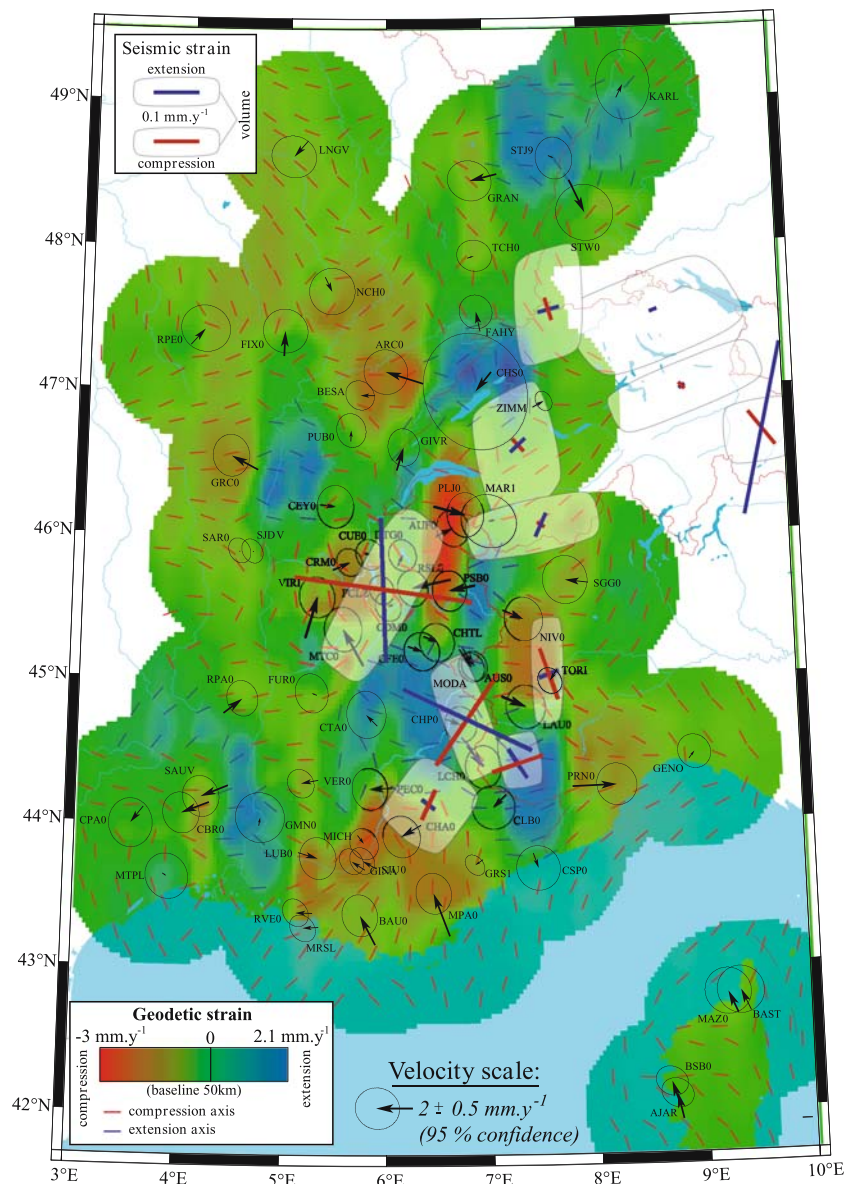
2.5D thin-shell finite element modeling

The 2.5D thin-shell finite element code SHELLS (Kong and Bird 1995; Bird 1999) solves stress equilibria and conservation of mass with presumed rheologies and densities. Models are built for a given 3D structure of topography and crust/lithosphere thickness. SHELLS solves the momentum equation in a vertically integrated form (2D approximation), corresponding to a ''2.5D finite element method''. This thin-shell approximation only allows solving the horizontal components of the momentum equation (the vertical component is replaced by the isostatic approximation), and no vertical shear traction is considered on vertical planes (i.e., flexural strength is ignored, elastic thickness is zero). The rheologies are modeled as anelastic, with thermally activated nonlinear dislocation creep in the lower crust and mantle and a Mohr-Coulomb frictional plasticity in the shallow parts of crust and upper mantle. Both a given initial surface heat flow and the assumption of steady state thermal conduction are used to compute the 3D temperature with constant but distinct heat production and conductivities for crust and mantle. Our models include 295 cells used in the finite element technique and has been described in detail by Delacou et al. (2005a). The boundaries of the models are designed to imitate the limits of the Western/Central Alps. At the eastern limit of the model, an arbitrary N–S running boundary has been fixed, with free tangential sliding behavior, limiting our study area to the Western/Central Alps (Fig. 8).
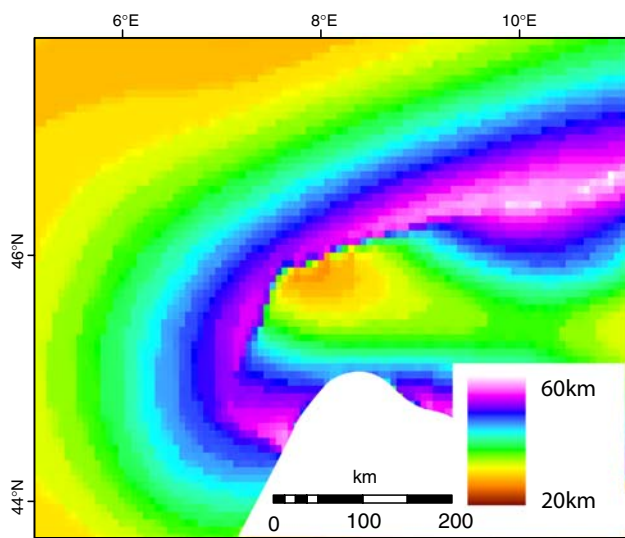
Fig. 7 Map of Alpine crustal thickness calculated from the Moho depth (Waldhauser et al. 1998) and average topography of the chain

To infer a realistic 3D crustal structure, we used a Moho geometry interpreted from wide-angle seismic experiments (Waldhauser et al. 1998). This results in a complex 3D-geometry, in which the highest topography is not directly overlying the crustal root.

The calculated stress field is characterized by radial fan-shaped extension in the regions of high topography and by radial fan-shaped compression in external zones. This pattern corresponds to GPA equilibration between regions of positive GPA in the inner areas and regions of "normal" GPA in external zones. This configuration leads to an extensional state of stress in the core of the belt, which tends to reduce overthickened crustal material, and in a compressive stress state in external regions in response to the extension of the inner areas. Our 2.5D numerical modeling, strengthened by the correlations with large-scale seismotectonic analysis, underlines the major role of body forces (GPA balance) in the current stress field of the Western Alpine Arc, and raises the issue of the still ongoing Europe/Africa convergence in Alpine geodynamics. The N- to NW-ward convergence, with an estimated 3–8 mm/year (e.g., Nocquet and Calais 2004) at the longitude of the Alps, could be accommodated in different areas between Europe and Africa, such as the Maghrebian belts, the Apennines, the Dinarides, and the Calabrian subduction. Our study suggests that no convergence is needed to explain the observed stress field of the Western/Central Alps, as it is mostly controlled by internal body forces.

2D crustal cross-section finite element modeling

The role of buoyancy forces in the Alps has been examined with another finite element code applied to the ECORS

profile on a crustal scale. The ADELI 2D-code (Hassani and Chéry 1996; Hassani et al. 1997) has been chosen, because it is able to model more complex and realistic rheologies: elastic (Byerlee 1978), elasto-plastic, visco-plastic, and viscous (Kirby and Kronenberg 1987). Our model involves a crustal section along the ECORS seismic profile, which has been gridded using about 7,000 elements (Fig. 9 a). The model has been built taking into account several interpretations of this section (Bayer et al. 1989; Nicolas et al. 1990; Roure et al. 1996; Burov et al. 1999; Schmid et al. 2004). The cross-section has been simplified in order to allow computing with the ADELI code. To satisfy the quasi-static condition implied by this code, the model has been built with a realistic crustal root below the topography. A major issue has been to equilibrate the dense Ivrea Body (d = 3.1; mantle material). The disequilibrium induced by the very high level of the Ivrea Body, imbricated within the upper crust, is compensated to some degree by the presence of low-density sediments (d = 2.4) in the overlying Po plain. The rheological parameters have been fixed using laboratory experiments of deformation (Kirby and Kronenberg 1987; Cloetingh and Burov 1996) as well as comparison with other tectonic numerical models (e.g., Chéry et al. 1990; Hassani and Chéry 1996; Burov et al. 1999; Cattin and Avouac 2000). The analyses of the different models tested show that modifications of these parameters within realistic ranges do not alter the major patterns of the stress/strain states.

The boundary conditions used in our modeling are the following: (1) An isostatic compensation surface located at 100 km depth within the mantle, without normal displacement, and with free tangential displacement. (2) A western surface without normal displacement, and with free tangential displacements. (3) An eastern surface with free tangential displacements and with a variable normal velocity. On this surface, we alternatively modeled fixed, compressive, and extensive boundary conditions. The temperatures used in this thermo-mechanical modeling are: 285°K at the upper surface and 1,473°K at the base of the model. The strain state J1 (ε) is visualized using a color code, with blue for extension and red for compression, while the stress Dev (σ) is represented by arrows.

Fixed boundary conditions

The normal velocity at the eastern surface is fixed to zero, with free tangential movements (as for the western boundary), and the evolution of the model is only due to gravitational potential adjustments. We observe an extensional area in the upper and lower crust below the over-thickened zone (topographic crestline), with a maximum intensity of strain/stress of about J1 (ε) = 1×10^4 and Dev (σ) = 3×10^7 Pa at the base of the upper crust. Compres-

Fig. 8 2.5D numerical models computed with the code SHELLS (from Delacou et al. 2005a). **a** Configuration of finite element grid of the presented model. We used a realistic crustal model computed with fixed boundaries. Main rheological parameters: mean density 2.816 (crust), 3.332 (mantle); fault friction 0.03; continuum friction 0.85; exponent of power law dislocation creep 3; shear stress coefficient 2.3×10^9 (crust), 9.5×10^9 (mantle). **b** Calculated stress fields; **c** Calculated surface velocities. Note the orogen-perpendicular stresses in an extensional mode in the core of the belt and in a compressive mode in the border areas. See text for details
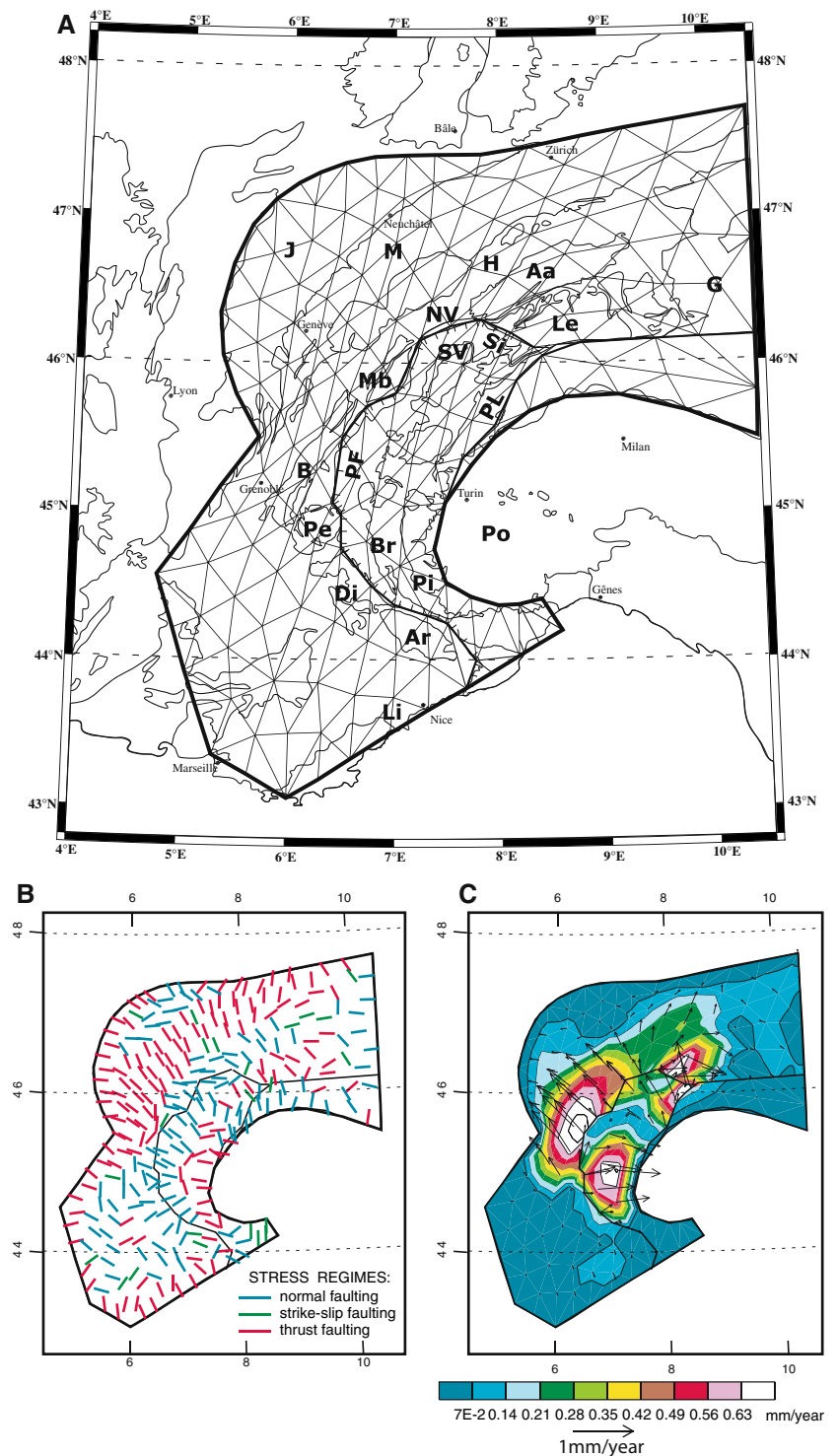
sive areas are observed in the forelands of the belt, with higher intensities for the eastern side [Po plain, J1 $(\varepsilon) = -0.7 \pm 10^4$ and Dev $(\sigma) = 2 \pm 10^7$] than for the western side [front of Belledonne massif, J1 $(\varepsilon) = -0.4 \times 10^4$ and Dev $(\sigma) = 1.5 \times 10^7$ Pa]. There is a complex zone

at the apex of the Ivrea Body. This complexity is caused by the isostatic adjustment between bodies of very different density. Given the simplicity of the geometric model, the results could be viewed as an artifact and we do not discuss its significance hereafter (Fig. 9b).
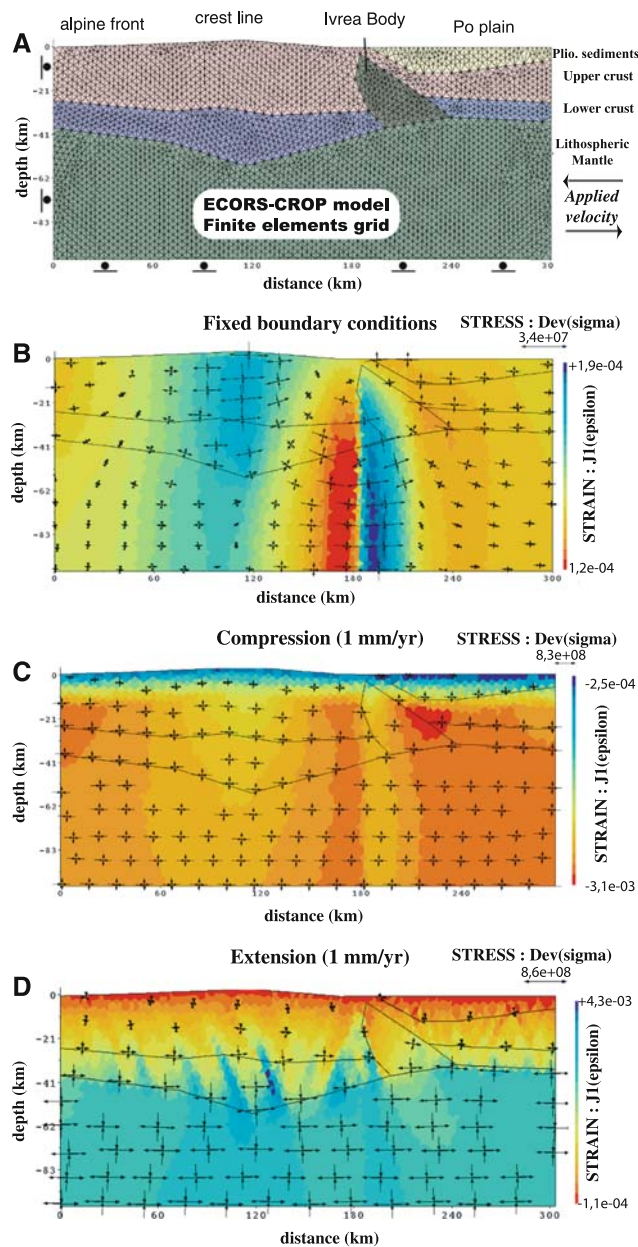
Fig. 9 2D numerical model computed with the code ADELI along a simplified ECORS cross section. Main rheological parameters used: Young modulus 1×10^{11}; Poisson ratio 0.25; internal friction coefficient 30; activation energy 137×10^3 (lower crust), 44×10^3 (mantle); exponent of power law dislocation creep 1.9 (lower crust), 3.35 (mantle). *Color code* gives the mode of deformation (extension in *blue*, compression in *red*); *small arrows* give the stress state. **a** Configuration of presented models, characterized by fixed left and bottom boundaries and a varying mobile right boundary. **b** Fixed boundary conditions; **c** Compressional boundary conditions; **d** Extensional boundary conditions. The contrasted seismotectonic configuration is well-modelled only by B (with extension in the core of the chain accompanied by compression in the external zones, see Fig. 5b) while a complex zone is found beneath the Ivrea body (due to its unstable isostatic position), with two bands of extension and compression. See text for details

Convergent boundary condition

We fixed the normal velocity on the eastern boundary to 1 mm/year toward the West. The obtained strain/stress states are convergent everywhere in the model. The maximum convergence rates are obtained in the convergent area of the first model [J1 $(\varepsilon) = -3.1 \times 10^4$ and Dev $(\sigma) = 8.3 \times 10^7$ Pa]. The extensional part of deformation seen in the first model has disappeared and replaced by very small velocities of convergence (of about 0.03 mm/ year); but overall, the qualitative state of strain/stress remains similar to the first model (Fig. 9c).

Divergent boundary conditions

We fixed the normal velocity on the eastern boundary to 1 mm/year toward the East (''lateral extrusion''). The obtained strain/stress states are now generally extensional in the entire model, except within the topmost 2 km, where a thin band of compressive stresses appears. This is an artIfact of flexural rigidity. The maximal divergent rates [J1 $(\varepsilon) = 4.3 \pm 10^4$ and Dev $(\sigma) = 8.3 \pm 10^7$ Pa] are obtained within steeply dipping shear bands (concentrated deformation). For smaller divergent velocities (of about 0.03 mm/year) we obtained an overall qualitative state of strain/stress similar to the first one, but dominated by extension (Fig. 9d).

Comparison with the seismotectonic regime

On a seismotectonic cross-section along the ECORS profile, the core of the belt is in a state of extensional deformation, affecting all of the upper crust below the crest line of the Alps, whereas the outer boundaries of the belt (forelands) are characterized by a moderate compressive regime, localized at the transition from high to low topography. This seismotectonic regime is best matched by the first model, with fixed boundary conditions, and GPA readjustments in the Alpine root. According to this model, buoyancy forces are sufficient to explain a major part of the active Alpine tectonics. Indeed, as soon as we introduce a small velocity due to plate tectonics, the contrast between the different tectonic regimes (extension versus compression) is lost.

Brittle Neogene tectonics

Morphotectonics and faulting

Landscape is the result of the interaction between tectonics, climate, and lithologies (e.g., Molnar and England 1990;

Molnar et al. 1993; Whipple et al. 1999). Tectonic forces are capable of modifying the hydrographic network (Jackson and McKenzie 1988; Van der Beek and Braun 1999; Burbank and Anderson 2001). A fault is a discontinuity along which fluid circulation and mechanical crunching have reduced rock strength (e.g., fault gouge and fault breccias). Because of this higher erodability, faults are often followed by rivers, creeks, gullies, passes or gentle slope variations, allowing their detection by remote sensing (DEM).

Here, we present an example of such a morphotectonic evolution from the Valais area. The present-day orientation of extension in the South Valais is almost N–S. It is different from the past mean $\sigma 3$ axes determined by paleostress inversion, which is ENE–WSW oriented (Champagnac et al. 2004). Figure 10 is an example of such a large fault, close to the ''Pas de Chèvres'' in the South Valais. The fault plane is oriented N170°/55°, with normal, down-dip striations in a thin veneer of hematite coating. The satellite image (IRS-1C, 3.5 m pixel size) displays this fault plane, which appears as a triangular facet with a 200-m long base (Fig. 10c, d). The topographic profile (Swisstopo DEM, 25 m pixel size) constrains the size and geometry of the fault plane: its vertical extension is almost 80 m, with a 50° dip. Small passes (spaced 200 m) in the northern part of the profile could be related to three other faults of comparable size and orientation.

The most remarkable geomorphic feature in the South Valais is the expression of the Rhône fault zone (RFZ). Although seismotectonic studies (Deichmann and Garcia-Fernandez 1992) show that the active Rawil fault zone is located several kilometres to the north, geomorphic features suggest a recent activity South of the Rhône valley: reverse slopes and flat areas can be followed along the Rhône valley for several tens of kilometres (especially between Sion and Sierre). A composite image, made with IRS-1C image (3.5 m pixel size) draped onto Swisstopo DEM provides a 2.5D view of this structure (Fig. 11 a). A kinematic analysis shows both normal and dextral components. Topographic profiles along crest lines show at least one reverse slope, related to lineaments running along the Rhône valley (Fig. 11b). The thickness of the associated fault gouge (Fig. 11c) as well as the ruptures in the slopes, are interpreted as the geomorphic expression of a quaternary long-lived normal and dextral RFZ. This geomorphic signature suggests an important displacement along this fault system, active up to recent times. The normal component along high angle, south-dipping faults would be responsible for topographic anomalies such as the observed counter slopes.

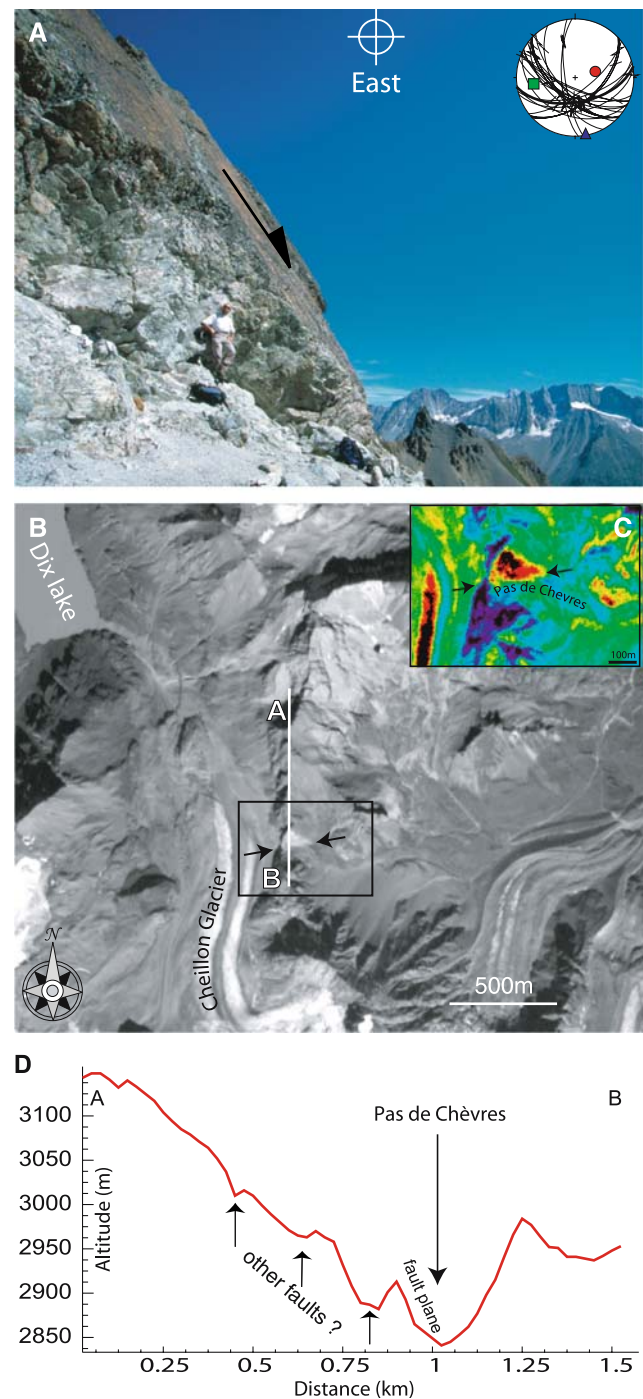For a complete analysis of the fault system in the Southern Valais, a map based on the alignment of

Fig. 10 Example of a several hundred meters long extensional fault scarp in the Southern Valais (''Pas de Chèvre'' fault). **a** View of the fault looking East. The fault plane is very slick, mineralized with hematite and striated with a normal component. The calculated paleostress tensor (*upper right*) exhibits a near-horizontal $\sigma 3$ axis (*blue*) oriented in a N–S direction. **b** and **c** IRS satellite images [panchromatic (**b**) and false colors (**c**)] of the same area. *Arrows* indicate the fault plane(triangular facet, in *red* and *black* on **c**) well recognized from space. The topographic profile AB in **d** shows the slope rupture corresponding to the main fault, and minor ruptures higher up on the ridge, probably, associated with minor normal faults
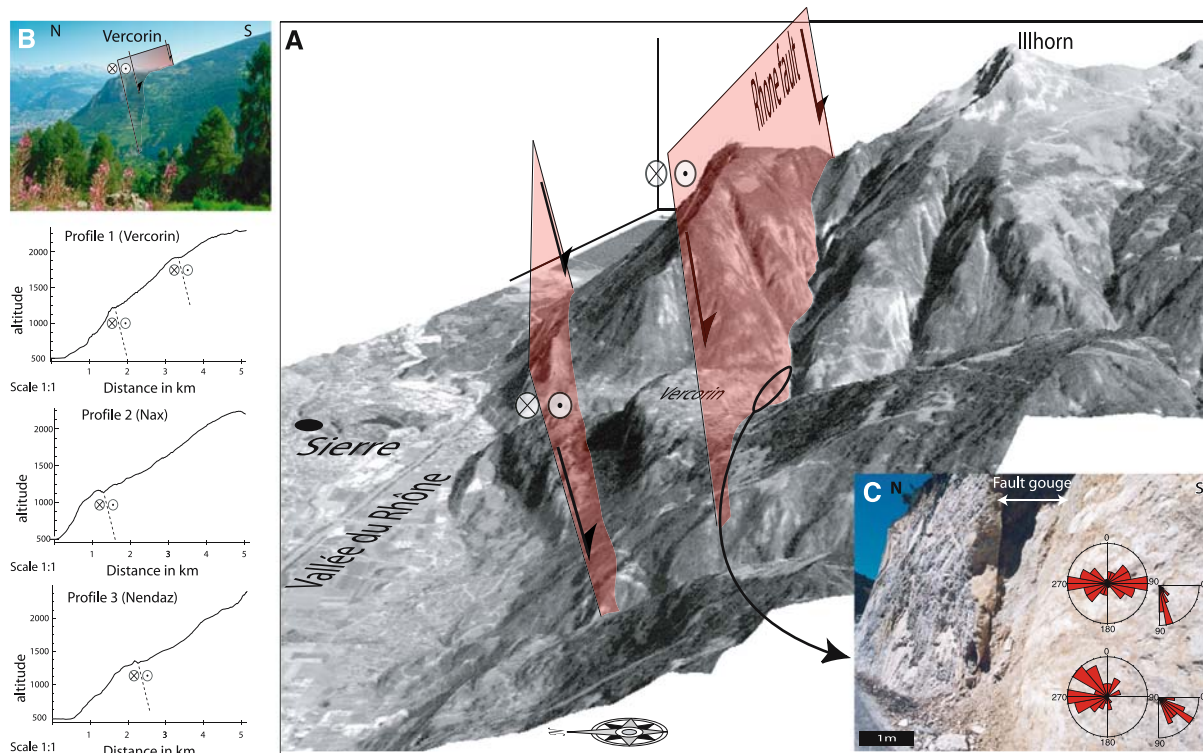
Fig. 11 Topographic expression of fracturing in the Southern Valais. **a** 3D interpretation of the observed fault pattern. The two major faults are shown in *pink*; they mark topographic slope ruptures reflecting normal faulting with a dextral component. **b** Topographic slope rupture (view toward the West) with the associated normal fault (*pink*), and N–S topographic profiles showing the slope ruptures associated with the Rhône fault in (**a**). **c** One meter thick fault gouge associated with the Rhône fault in (**a**). Stereo plots display the orientation and the dip of associated minor faults. Their general E–W orientation is compatible with the orientation of main topographic lineaments observed in (**a**)

high-frequency slope ruptures was constructed. Figure 12 a illustrates slope orientations and the slope values with color contrast. This characterization of slopes allows the detection of linear slope variations. Reverse slopes are particularly emphasized (see for instance between Sierre and Sion immediately South of the Rhône). Because alignments of slope variations are strong indicators for faults, especially if they run across a crest or a valley, the map of linear slope variations can be regarded as a fault map (Fig. 12b). In many places, the faults were verified by fieldwork (Bistacchi et al. 2001; Champagnac et al. 2003). The map was manually drawn, with neither automatic detection nor extrapolation, and shows about 500 faults varying from 400 m to 10 km long. Three directions were detected at this scale (inset in Fig. 12b).

The main direction is NE–SW, and is related to the RFZ (Champagnac et al. 2003 2004), with normal and dextral movements under the current stress field. This direction is poorly expressed at the outcrop scale, but its geomorphic expression is striking, especially close to the Rhône valley. Four similar fault strands (ca 10 km spacing) run further south (Fig. 12b). The E–W direction is also related to the RFZ; it could also be related to the Aosta Fault System to the South (Bistacchi et al. 2001) and to the Insubric Line (Schmid et al. 1987). Kinematic analyses indicate mainly dextral movements, with a normal component. The NW–SE direction is less important at this scale. It is, however, the most strongly expressed direction for outcrop-scale faults. It is clearly related to normal faulting with a sinistral component. The two first families are compatible with the current stress field and with previous studies (cf. Burkhard 1988), whereas the third one is mostly related to outcrop-scale faults and the associated stress field (Champagnac et al. 2003). The NW–SE direction is similar to the main river directions; deep incisions of their valleys (locally up to 2,000–3,000 m) suggest that the related faults are old; they record extension related to the Simplon fault and the Neogene stress field.

Orogen-parallel versus orogen-perpendicular extension

We present in this section a synthesis of the brittle deformation analyses conducted over the last decade within the bend of the Western and Central Alps. Paleostress fields have been computed using the direct inversion method of Angelier (1990). There is an ongoing debate about the

Fig. 12 Fault identification by geomorphic analyses using Swisstopo 25 m DEM. **a** Representation of slope values (*saturation*) and slope directions (*color*) used in the detection of topographic lineaments associated with faults (also controlled in the field). **b** Fault map derived from the DEM analysis. The main direction of faults (*bottom right*) is oriented NE–SW, whereas minor faults trend E–W and NW–SE
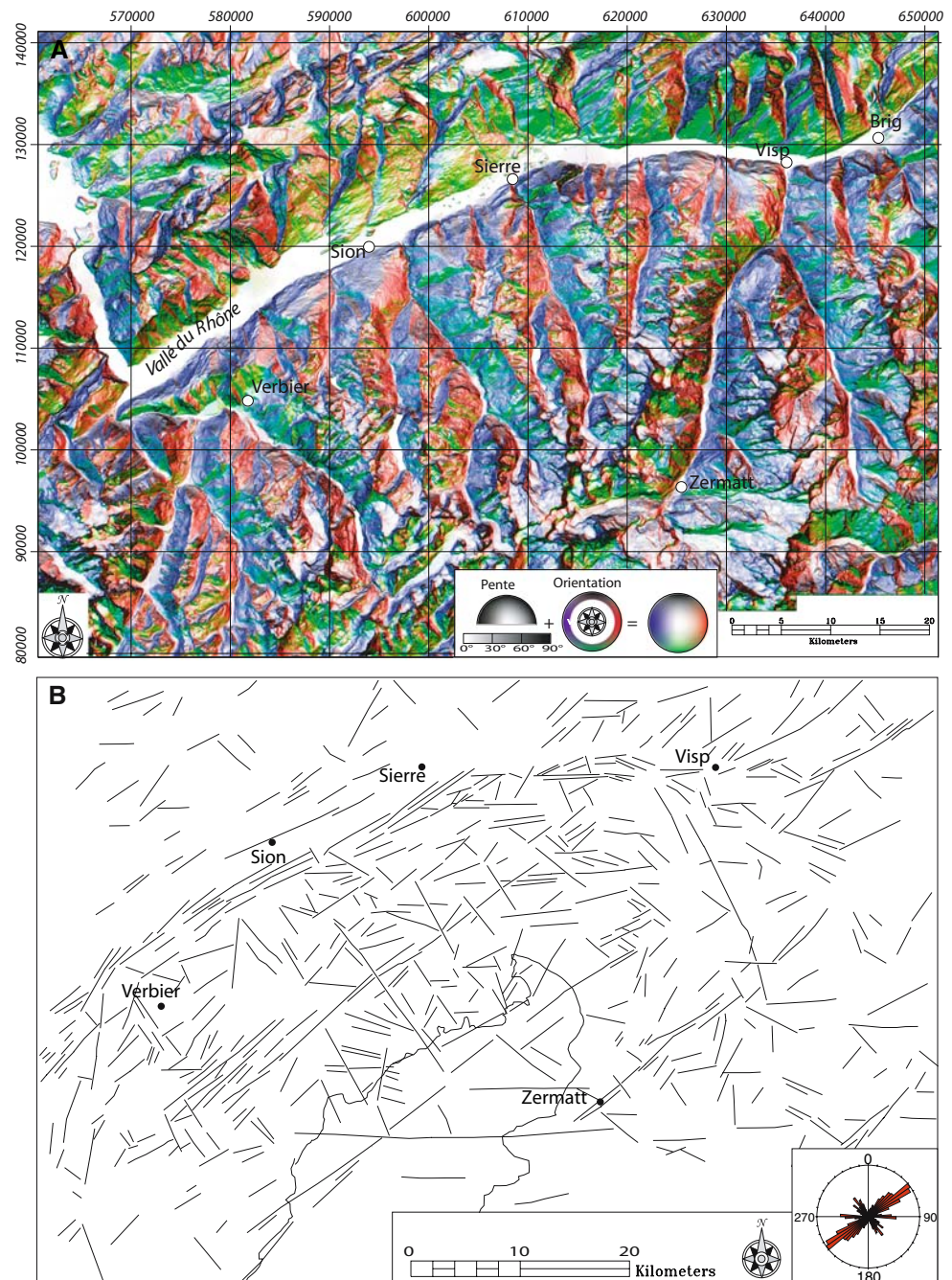
significance of such inversions and the associated terminology of stress versus strain (e.g., Marrett and Peacock 1999). Regardless of this somewhat semantic issue, we deal with the reconstruction of the stress state acting within the belt since Early Miocene times. A series of regional analyses has been incorporated into our large-scale synthesis (Champagnac et al. 2003, 2004; Grosjean et al. 2004). This provides a large and rather homogenous database (312 paleostress tensors) covering the entire arc of the inner Western and Central Alps, corresponding to a surface of some 10,000 km^2 (average density of 3 tensors/100 km^2).

We refer to Champagnac et al. (2006) for the parameters of these paleostress tensors. Faulting systematically overprints ductile compressional structures (folds, nappe piles, schistosities). Thus, this brittle deformation has been qualified as "late Alpine faulting", reflecting Mio-Pliocene tectonics (Fig. 13).

The most frequently observed brittle deformation structures in the inner Western Alps are extensional faults (Fig. 14 a). More than 7,000 individual meso-scale normal faults have been measured all around the Alpine Arc. We also measured about 1,000 transcurrent faults, which ap-

pear to be closely linked to the extensional ones, as discussed below.

Figure 13 presents examples of such normal faults, and related meso-scale and large-scale structures. Numerous other examples of such extensional and transcurrent late Alpine structures have been published in the Western and Central Alps (e.g., Sue and Tricart 2002, 2003; Champagnac et al. 2003, 2004; Grosjean et al. 2004). At first sight, the overall pattern of the σ3 axes (Fig. 14b) corresponds to a striking orogen-parallel extension, which is very stable all along the Alpine Arc from the Simplon to the Ubaye area. A continuous change in σ3 direction is documented from N065° in the Simplon and Valais areas, to N–S in the Vanoise area and to NNW–SSE in the Briançon area. The dispersion of the σ3 axes is very small in the Simplon area, probably because of a strong kinematic control by the major Simplon fault zone. The dispersion of σ3 axes is increasing southwestward, but the direction of extension parallel to the orogen remains well constrained. Another

striking characteristic is the increasing number of orogen-perpendicular σ3 axes from the North to the South (Fig. 14c). This orogen-perpendicular extensional stress pattern appears as a second-order signal. It could be associated to a second phase of late extension in the Alps. In the Briançonnais area, the reactivation of the crustal Penninic thrust as an extensional detachment (see above) seems to be at the origin of the E–W to NE–SW oriented σ3. It is similar to the present-day stress field inferred from seismotectonics, which suggests that the orogen-perpendicular extensional stress field was established after the orogen-parallel one.

Beyond the widely developed parallel extension and the current perpendicular extension presented above, part of the extension documented in the Western Alps corresponds to early normal faulting, perpendicular or oblique to the belt and often developed at the brittle-ductile boundary (e.g., Rolland et al. 2000). These early extensional structures could be linked to the relative uplift of the ICM. The

Fig. 13 Relative chronologies observed in the field. a Metric E–W trending normal faults cutting across strongly folded amphibolites (Valpelline, Val D'Aosta) reflecting NE–SW extension (blue axis). b Striated faults used in our paleostress analysis. Polyphase faulting is reflected by cross-cutting faults and superposed striae (Mont-Cenis, Haute Maurienne). A detailed analysis of this area reveals a first NNE-SSW extension, then a strike-slip regime with σ3 oriented E–W. Such strike-slip movements are often observed together with typical normal fault geometries
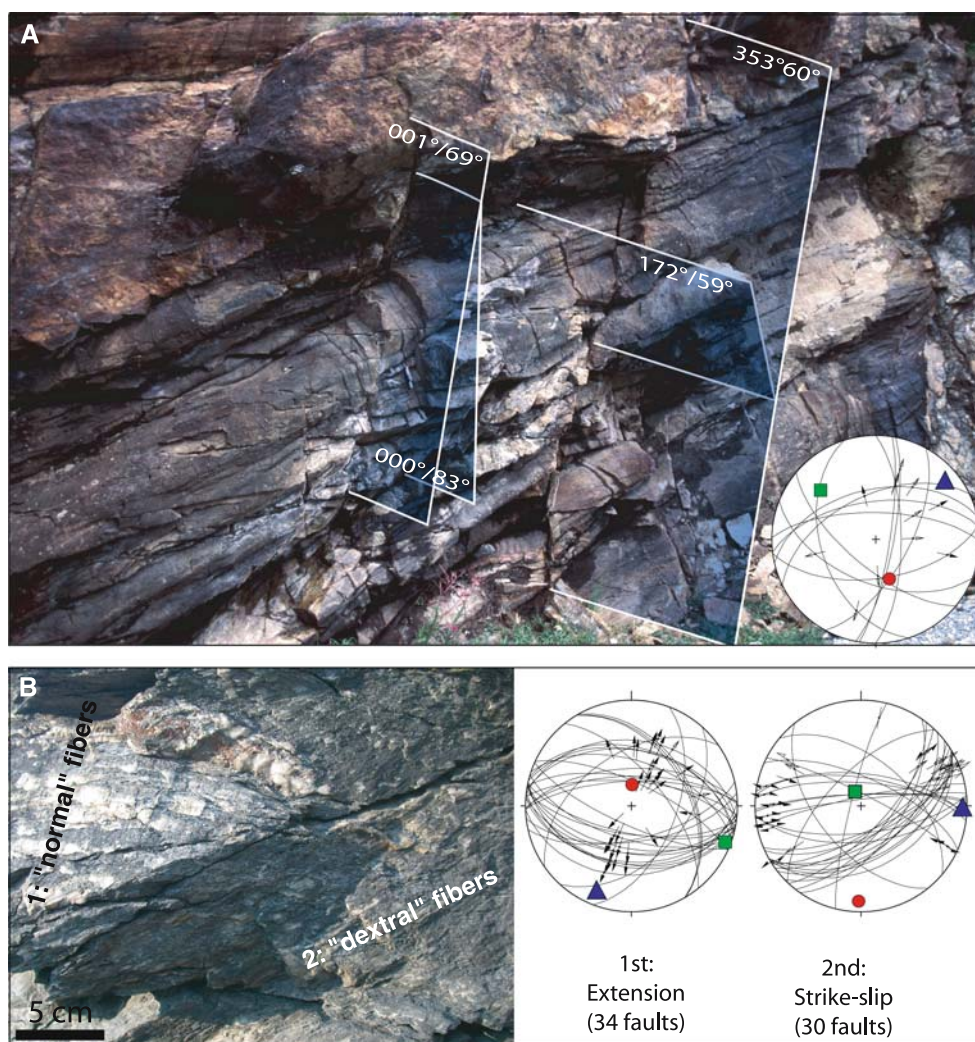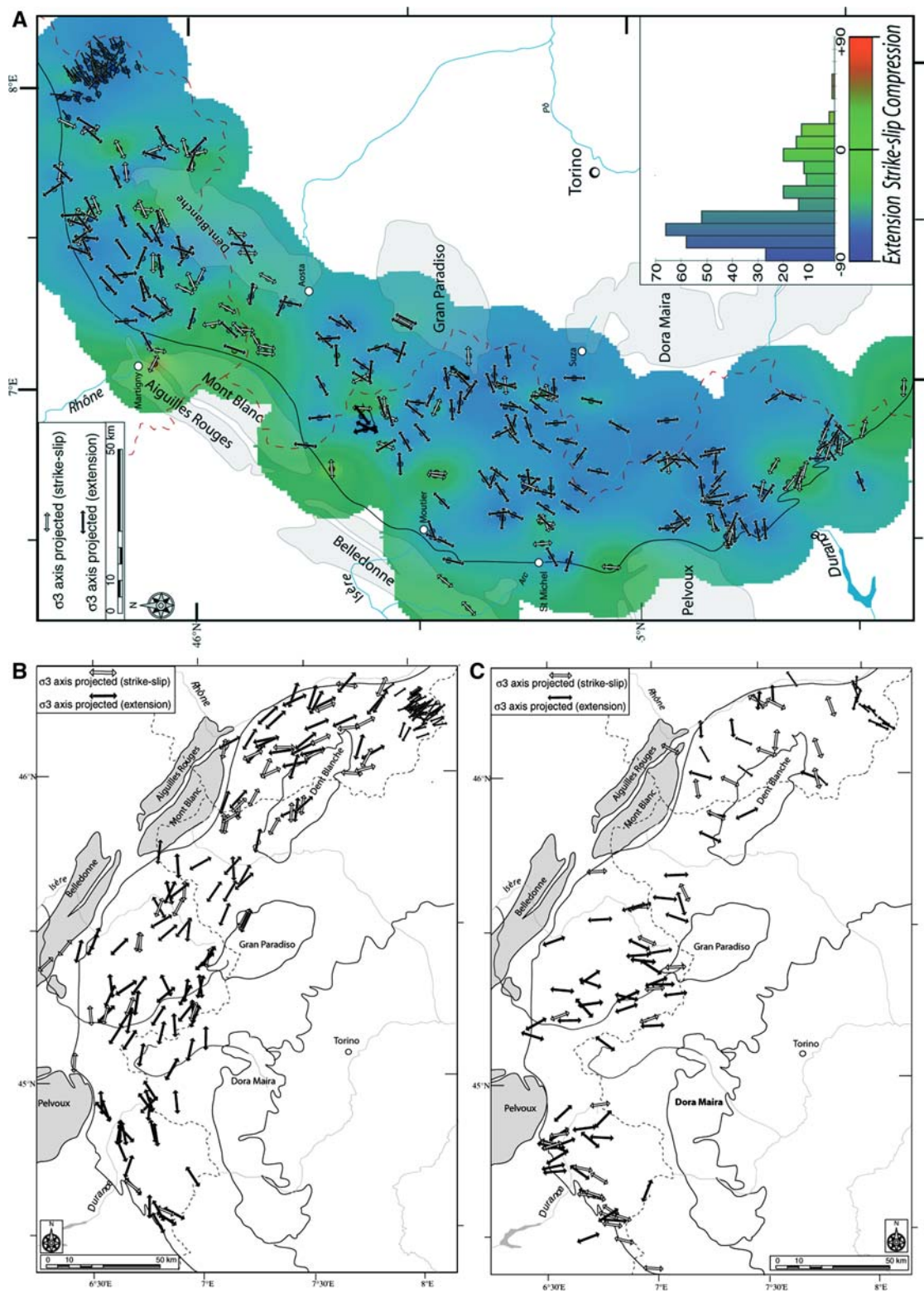
Fig. 14 Synthetic paleostress map covering the western internal Alpine belt (from Champagnac et al. 2006). More than 300 paleostress tensors are represented, corresponding to about 6,000 fault measurements. **a** σ3 directions of extensional (*black arrows*) and strike-slip (*white arrows*) tensors. The *background color* shows the tectonic regime derived from the calculated tensors (*same colors* as in Fig. 4), which is mainly extensional (*blue*). **b** Major directions of extension oriented in an orogen-parallel direction with respect to the Alpine arc (Mio-Pliocene). **c** Minor directions of extension oriented in an orogen-perpendicular direction (Pliocene-recent, compare with Fig. 4). See text for details

exhumation of the ECM may also have led to similar early extension, in particular close to the CPF (Cannic et al. 1999; Seward and Mancktelow 1994).

Transcurrent versus extensional tectonics

On average, the percentage of transcurrent versus extensive paleostress tensors is around 25% versus 75%. Accordingly, the transcurrent stress field appears to be less recorded by brittle deformation, superimposed on a first-order extensional regime. In order to represent the relative importance of the transcurrent versus extensional brittle tectonics within the internal Western Alps, we calculated a scalar variable r depending on the plunges of the $\sigma 1$ and $\sigma 3$ axes. The interpolation of this parameter allows drawing a regionalized map of the deformation (background Fig. 14 a). This map displays a predominance of an extensional state of paleostresses (blue). Strike-slip (green) is observed in some places, especially in the westernmost part of the studied area, and on the eastern side of the Mont-Blanc massif. This zone of transcurrent deformation separates the Alpine Arc into two extensional areas, the Simplon/Valais areas to the North, and the Vanoise/Briançon area to the South.

The relative chronology between extension and strike-slip is well established at many sites. Extensional deformation is regionally older than the transcurrent one in the southern part of the belt from the Ubaye massif to the North-Vanoise area. In contrast, extension appears to be younger than strike-slip in the Valais area. These two sectors are separated by the Aosta valley, where transcurrent tectonics dominates. This observation raises the issue of the specific role of this area in the late evolution of the belt.

A statistical analysis of $\sigma 3$ directions performed all around the belt by Champagnac et al. (2006) revealed a remarkable stability in the region $\sigma 3$ directions both for the extensional and transcurrent paleostress fields. The $\sigma 3$ direction remains stable in the whole belt, even when extension turns into strike-slip and vice versa. Accordingly, we suggest that the temporal switching between $\sigma 1$ and $\sigma 2$ axes took place during a single overall extensional to transtensive ''deformation phase'', with only local instabilities in space and time modifying the specific stress field (Champagnac et al. 2006). Such permutations of stress axes could also be induced by rock heterogeneities and anisotropies (Hu and Angelier 2004).

Timing of brittle deformation

Direct dating of brittle deformation remains difficult and there are virtually no data available for the Western Alps. Nevertheless, relative dating with respect to Alphine compressive structures allows to better constrain the age of faulting within the Alpine Arc. Late Alpine faults postdate Alpine metamorphism and related ductile deformation (Fig. 13). We assume brittle extension to start near the ductile-brittle transition at around 300°C at a depth of ca 10 km (Scholtz 1990; Guéguen and Palciauskas 1992; Sibson 2003). Thus, the brittle structures observed were formed in the uppermost 10 km of the Alpine crust. The observation of very slick planes and the presence of thick layers of fault gouges suggest brittle deformation within the topmost 4 km of crust, at temperatures below ca 120°C (Scholtz 1998; Sibson 2003). The very complex exhumation processes in the Alps, the lithological variations and the various strain rates do not allow to give an approximate age for specific locations of the ductile-brittle transition in the belt. Nevertheless, according to Malusa et al. (2005), such a transition should have occurred as early as in late Oligocene to early Miocene times in the internal Alps. To summarize, late Alpine faulting exhibits two directions of extension. The dominant extension direction is orogen-parallel throughout the Neogene. The present-day regime of orogen-perpendicular extension seems to have been initiated only in relatively recent times.

Geodynamic interpretations

Extensional tectonics is described from numerous mountain ranges (e.g., Ménard and Molnar 1988; England and Houseman 1989). Geodynamic models of post- or syn-orogenic extension examine the complex interplay between intrinsic body forces (buoyancy) and extrinsic boundary forces (plate tectonics). The temporal evolution of the delicate equilibrium between these forces is held responsible for the dynamic and kinematic evolution of orogens, including extensional processes. In the Alps, we established two extensional phases. The first one corresponds to an orogen-parallel extension that affected the inner Alpine Arc during Neogene times. The second one, perpendicular to the belt, is still active today and may have developed from the Pliocene onward. In this section we discuss the related geodynamic models.

Orogen-parallel extension

Most of the extension observed in the inner Western Alps is oriented parallel to the strike of the belt and follows the overall bend of the Alpine Arc. This extension was taking place contemporaneously with compression, folding, and thrust propagation observed in external zones to the north, west, and southwest. This observation alone allows discarding simple post-orogenic collapse models. Many syn-orogenic extension models, proposed for cross-sections in a convergent context, imply an extensional direction within a 2D section parallel to the shortening one (Fleitout and

Froidevaux 1982; Molnar and Lyon-Caen 1988; England and Houseman 1989; Jolivet et al. 1998). These 2D cases do not apply to the Western Alps, where extension is taking place at a high angle to shortening, subparallel to the belt. Given the strongly curved shape of the Western Alps, extension could be seen as a 3D effect of ''outer-arc-stretching'' (Burg et al. 2002), ''vertical indentation'', or a ''transtension in an overall compressional orogen'' (Hubbard and Mancktelow 1992; Steck and Hunziker 1994); however, the lateral consistency of arc-parallel extension observed within the entire belt remains difficult to explain in all these models.

An alternative class of models calls for ''lateral extrusion'' of crustal or lithospheric blocks in a collisional context. Numerical modeling by Seyferth and Henk (2004) demonstrates that such lateral extrusion is to be expected during late orogenic evolution, even in cases of moderate to small crustal thickening. Regardless of the boundary conditions, all the models of Seyferth and Henk predict orogen-parallel extension in the range of 10–70% of shortening. In models with a free boundary, such as an opening basin, extrusion is facilitated and accordingly the percentage of extension is increased. This class of models goes back to the proposal made by Molnar and Tapponnier

(1975) for Tibet, and has subsequently been applied to the Eastern Alps (Tapponnier 1977; Ratschbacher et al. 1989), and Turkey (Dewey et al. 1986; Le Pichon et al. 1994).

We propose that a similar geodynamic process ruled the large-scale orogen-parallel extension observed within the Western Alps (Fig. 15). The Ligurian Sea, which opened during Early Miocene times, plays the role of free boundary of this system to the South. The strongly arcuate geometry of the southern tip of the belt would eventually have blocked lateral extrusion there. However, the final geometry as seen today was only acquired very lately in Alpine history. An important late modification was induced by the retreating Apenninic slab in Late Miocene to Pliocene times (Gueguen et al. 1998; Rosenbaum and Lister 2004b). Apatite fission track data document exhumation and cooling ages of the Argentera massif and the Ligurian Alps at 11 Ma, with an acceleration at 5 Ma (Bigot-Cormier et al. 2000; Bogdanoff et al. 2000; Foeken et al. 2003). The 11 Ma age corresponds to the transfer of extension from the Ligurian Sea to the Tyrrhenian (Kastens and Mascle 1990; Rollet et al. 2002). In short, the Alpine geometry in Middle Miocene times is compatible with a southern free boundary (of the Ligurian Sea) in the direct prolongation of the high chain of southernmost Western
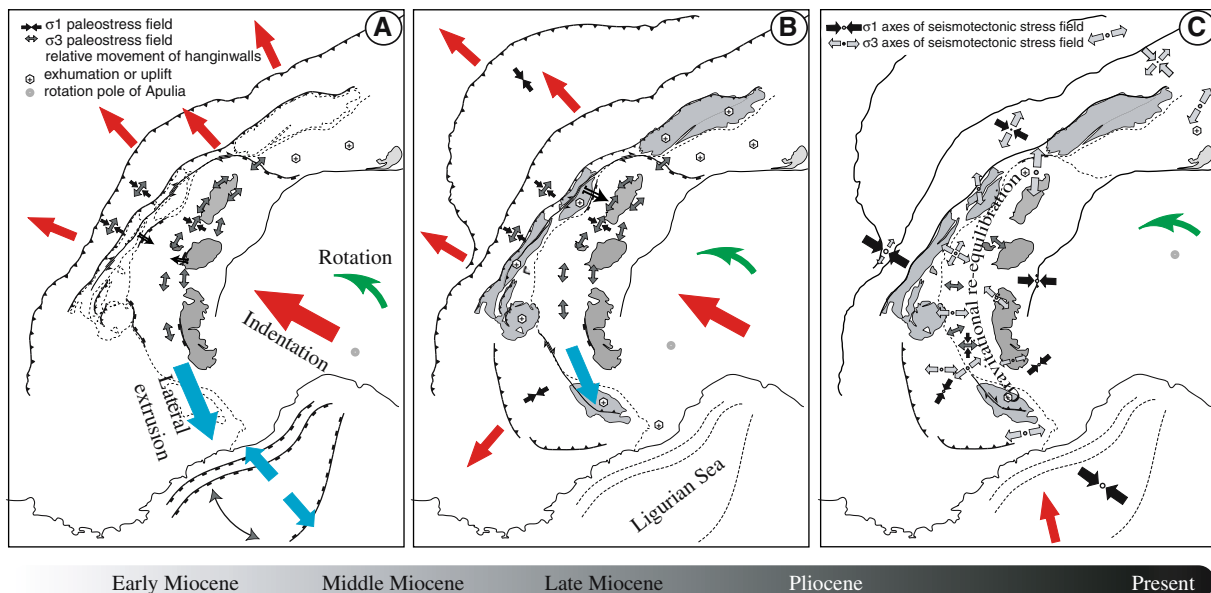

Fig. 15 Schematic tectonic sketches showing the Neogene geodynamic evolution of the Western and Central Alps. **a** Early to Middle Miocene: the propagation of the compressive Alpine front starts to affect the external, European domains (Helvetic zone) while the opening of the Ligurian basin to the south provides a free boundary enhancing the lateral escape of the internal areas of the belt toward the south. The main direction of extension in the internal zones is orogen-parallel. **b** Late Miocene to Early Pliocene: the compressive front is propagating toward the external domains, reaching the Jura Mountains and the Digne nappe system. Although opening of the Ligurian basin ceased, the southern termination of the belt still plays the role of a free boundary enhancing the lateral escape of the internal Alpine areas and the development of orogen-parallel extension. **c** Pliocene to present-day: the indentation of the Adria plate with Europe decreases. The role of gravitational body forces becomes predominant, and the core of the belt is now affected by orogen-perpendicular extension, while the Ligurian basin now undergoes compression. The role of rotational boundary forces, in all sketches, is indicated by a *green*, *curved arrow* in the Po plain area. The rotation of Adria induced, particularly in recent times, the evolution of a dextral fault system along the western border of the belt

Alps. One of the most important objections often raised against an ''extrusion model'' for the Western Alps, is the lack of any major left-lateral fault system along the eastern boundary of the system; a dextral strike-slip system, however, has been described above. This leads to a third class of models, which invokes the counterclockwise rotation of the Adriatic plate (Fig. 15), with a pivot close to the center of the Western Alpine Arc, i.e., within the Western Po plain (e.g., Laubscher 1991).

Hubbard and Mancktelow (1992) were the first to propose lateral extrusion in association with major SW extension observed at the Simplon fault, and strike-slip along the RFZ. In their model, internal units of the Western Alps would be transferred toward the Southwest and the flysch nappes (Embrunais-Ubaye). A comparable model was also discussed by Bistacchi et al. (2001) for the Aosta valley. Our own results indicate that the extensional deformations developed much further toward the South and the Southeast, and we therefore propose a semi-rigid block bounded by the Simplon normal fault to the Northeast, the Rhône and the Belledonne-Mont-Blanc right-lateral faults to the North and the West, and the equivalent right-lateral high-durance–SBF system to the Southwest. The eastern limit of this internal extruding block still remains undefined. This model allows explaining most part of our observations and fits quite well with the overall Alpine context during Miocene times.

Ongoing orogen-perpendicular extension

There is a close correlation between the tectonic mode of active deformation and crustal thickness. Extension is located at the apex of overthickened crust, all along the crest line of the Western and Central Alps, whereas compressional deformation is limited to a few areas along the outer borders of Alpine relief. To explain this tectonic contrast, we propose a geodynamic model dominated by buoyancy forces within the Alps including the root of the belt. In this model, active extension is explained as an effect of isostatic re-equilibration of crustal volumes. The high chain (crustal thickness up to 50 km) tends to collapse with respect to the West-Alpine foreland and the Po plain (crustal thickness of around 30 km). Basically, this post-orogenic regime would result from the reorganization of the gravitational potential within the Alpine belt. A counterclockwise rotation of the Adriatic plate could locally induce a reorientation of stress/strain axes and explain the predominance of right-lateral motions observed all around the western side of the belt. This model has been tested using numerical modeling (see above), which showed that the observed tectonics is best matched by fixed boundary conditions without any external forces applied. GPS surveys and seismic strains confirm the absence of significant

movements across the Western Alps. In summary, we propose a post-collision model for the present state of the Western and Central Alps mainly controlled by body forces in the Alpine root.

Many details remain to be quantified, however. Significant present-day uplift rates (up to 1.5 mm/year) are documented for the internal Swiss Alps (with respect to the immediate foreland). Areas with high uplift rates seem to correlate with the seismically most active extensional zones, both in the South Valais and Grisons (Gubler et al. 1981; Kahle et al. 1997). In our model, this correlation between high chain (thick crust), extension, and uplift is explained by isostatic readjustments through extensional tectonics, leading in turn to uplift. However, uplift may also be induced by other processes such as high erosion rates (Champagnac et al. 2007), post-glacial rebound, and/or lithospheric processes such as slab break-off (see below) and associated thermal effects within the mantle and lower crust.

Late Alpine tectonics and geodynamic implications

During Neogene times, Alpine tectonics was characterized by widespread orogen-parallel extension in the internal zones, coeval with the westward propagation of the compressive front in the external zones. This regime is interpreted in terms of lateral extrusion of the internal zones to the South where the Ligurian Sea was opening along the western side of the Adriatic promontory, indenting into the European plate. In contrast, recent deformation is characterized by orogen-perpendicular extension, which affects the high chain as a whole, whereas the most external zones are undergoing a right-lateral transcurrent regime, with local compressional areas. This deformation pattern is interpreted in terms of a post-collisional regime, in which convergence between the Adriatic and Europe plates had come to a halt. The present-day regime is dominated by intrinsic body forces within a still substantially overthickened crust. Rotational boundary conditions explain the importance of right-lateral strike-slip all around the Alpine Arc. These two tectonic regimes are fundamentally different; they result from the interaction in time and space of different geodynamic processes within the Alpine realm (Figs. 16, 17). We list hereafter the main processes, which must have had an influence on the late Alpine tectonic evolution.

Boundary conditions

Convergence and collision

The collision between Adria and Europe is responsible for the formation of the Alpine belt. Tethyan subduction started in Late Cretaceous/Eocene times and resulted in
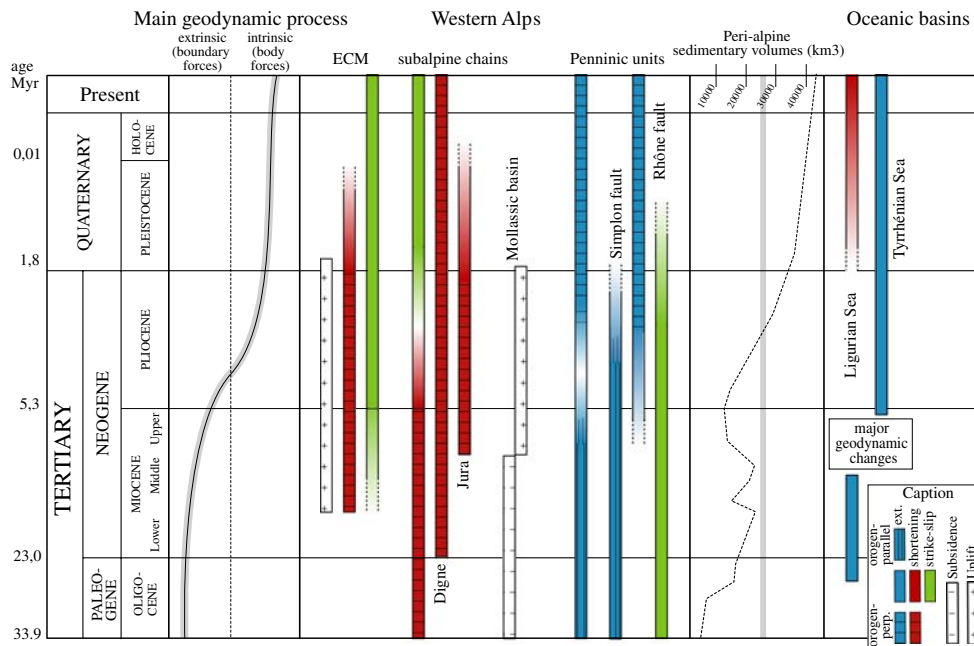
Fig. 16 Synthetic diagram showing the tectonic evolution of the Alpine belt and its periphery and the associated geodynamic processes. The color code represents the tectonic regime affecting the different domains of the belt through time. *Horizontal* or *vertical* lines within the *colored bars* show the orientation of the principal horizontal axes of deformation that are orogen-parallel or orogen-perpendicular. The *left curve* (equilibrium between boundary forces and buoyancy forces) documents the important role of decreasing convergence in the development of gravitaty-related, orogen-perpendicular extension in the core of the belt. The *right curves* represent the amount of sediments derivated from the Alpine chain and deposited in peripheral basins (Kuhlemann et al. 2000). The Pliocene increase in sedimentation reflects increasing erosion of the belt, possibly enhancing (directly or indirectly) orogen-perpendicular instead of orogen-parallel extension

Fig. 17 Conceptual diagram showing the interactions between intrinsic (*rectangles*) and extrinsic (*ellipses*) forces leading to the development of orogen-parallel versus orogen-perpendicular extension. The major roles are attributed to boundary conditions (convergence, lack of convergence, free boundary) and their equilibrium with gravitational re-equilibration (body forces)
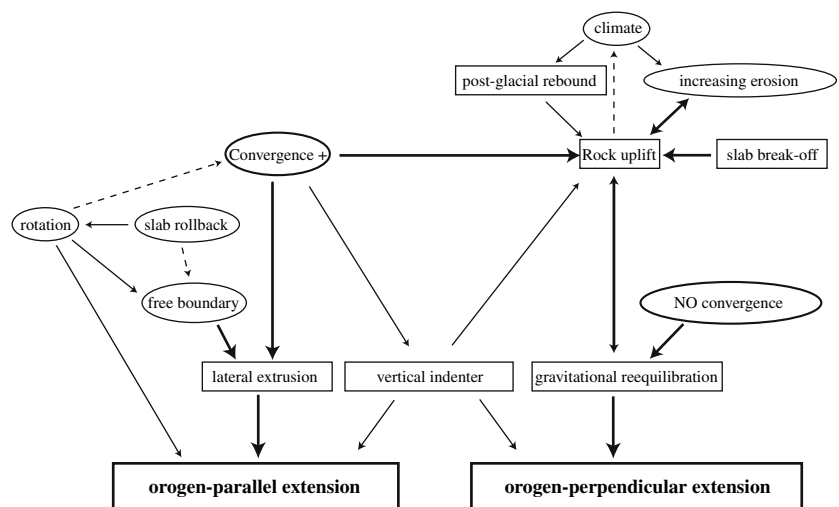
overall collisional shortening of about 120 km since Oligocene times (Schmid and Kissling 2000). The last steps of this convergence resulted in the evolution of the Jura fold-and-thrust-belt (Sommaruga 1999). At present, GPS measurements do not show any convergence across the Alpine Arc. An important slow-down and finally a complete halt of convergence must have taken place in the Western Alps at some ill-defined time in the Late Miocene or Pliocene.

Rotation

The counterclockwise rotation of the Adriatic plate since the Late Oligocene is a major factor in the formation of the

present-day structure of the Western Alpine Arc (Gidon 1974; Ménard 1988; Vialon et al. 1989; Laubscher 1991; Schmid and Kissling 2000; Collombet et al. 2002). At present, this rotation may be going on, albeit with a low velocity around a pole close to Milano (Anderson and Jackson 1987; Calais et al. 2002). This rotation explains the predominance of right-lateral motion observed all around the belt. However, the size and shape of blocks taking place in this rotation and the associated kinematics are difficult to assess.

Opening of the Ligurian Sea

The opening of the Ligurian Sea with the displacement of the Corsica-Sardinia block during Early Miocene times had a strong influence on the Alpine Arc at its southern termination. It resulted in the oceanization of the basin during Middle Miocene times (Carminati et al. 1998; Rollet et al. 2002; Rosenbaum and Lister 2004a). At present, the Ligurian Sea margin is characterized by a compressive regime, leading to the tectonic inversion of Miocene extensional structures (Béthoux et al. 1992).

Deep dynamics

Gravitational buoyancy forces

Post-orogenic gravitational re-equilibration may explain the recent extension in the Alpine Arc. Its dynamics are ruled by buoyancy forces within the belt, which became predominant with the decrease and halt of the convergence between European and Adriatic plates (Fig. 16). This class of model invokes gravitational collapse and spreading of an overthickened crust to explain extension (e.g., Ménard and Molnar 1988; Molnar and Lyon-Caen 1988; Selverstone 2005).

Slab dynamics

Slab break-off or partial slab break-off of the Tethyan lithosphere has been proposed as the driving force for thermal and extensional tectonic events in the Alps during Oligocene times (Von Blanckenburg and Davies 1995; Marchant and Stampfli 1997; Stampfli et al. 1998). Tomography reveals a complex slab configuration below the Alps (Lippitsch et al. 2003; Spakman and Wortel 2004). The geometry and the dynamic evolution of the remaining Alpine slabs have a strong influence on the Alpine geometry as seen at the surface today (Lippitsch et al. 2003). Topography and the present-day tectonic regime of the Alps are intimately linked to deeper processes such as slab retreat, cold slab-related material being replaced by warmer asthenosphere in the case of slab tear

and break-off. Times scales of millions of years are to be considered in the re-equilibration of the deep thermal structure of the overthickened crust and underlying mantle.

Vertical indentation

Vertical motion of a deep indenter in a compressive context has been proposed to explain the extension observed locally at the ductile-brittle boundary in the internal Western Alps (Rolland et al. 2000; Wawrzyniec et al. 2001). Such a model would imply a very important decoupling between deep and shallow Alpine structures, as it would imply large-scale compression, which is not documented by geodetic measurements (see above). Such a decoupling appears unrealistic in the recent Alpine geodynamic context.

Surface processes

Erosion

A Pliocene increase in the erosion rates has been deduced on the basis of sedimentary fluxes, quantified for peri-Alpine basins and deltas (Kuhlemann et al. 2002; Kuhlemann and Kempf 2002). As such a tendency is observed worldwide (Zhang et al. 2000). It seems to be driven by a global change in climate. The onset of glaciations, together with major changes in oceanic and/or atmospheric circulation patterns, would have led to an increase in erosion rates. Such an increase in erosion rates may in turn have had an important impact on the geodynamics of the Alps (Champagnac et al. 2007), as it transfers large volumes of rocks from the high chain to the periphery of the orogen and induce rock uplift by isostatic compensation (Cederbom et al. 2004).

Post-glacial rebound

Isostatic rebound after the retreat of Alpine glaciers some 19,000 years ago (Ivy-Ochs et al. 2004) has widely been discussed (Schaer and Jeanrichard 1974; Gudmundsson 1994; Persaud and Pfiffner 2004); however, quantification of this factor remains difficult. A sensitivity study by Gudmundsson (1994) shows that post-glacial elastic rebound might well be a significant component of the present-day vertical tilt rate of 1.5 mm/year observed between the inner Alpine valleys (Valais) and the Alpine foreland. The disappearance of the large Alpine glaciers should have provoked generalized uplift as observed in Scandinavia (e.g., Klemann and Wolf 1998; Wu et al. 1999). Such a rebound, if still active, should induce uplift mainly in the areas of maximum ice thickness (e.g., Kelly et al. 2004) and may

actually be integrated in a more general isostatic uplift of other origin.

Discussion

Interactions between the different geodynamic processes control the balance between intrinsic and extrinsic dynamics and explain the late tectonic evolution of the belt. Figure 17 presents a synthesis of the tectonic observations and the links with the related geodynamic engines involved in the Neogene to present evolution of the Western and Central Alps. Three main processes seem to play a fundamental role in this tectonic evolution. First, the end of the opening of the Ligurian Sea during Late Miocene times would imply a decrease in orogen-parallel extension. Second, a progressive decrease in the rate of continental collision (Europe-Adria) appears to be critical for the change of tectonic regime. Extrusion models imply convergence. The decrease of convergence rates allows buoyancy forces to develop that control the actual gravitational spreading. Third, the increase of erosion rates during Pliocene times probably corresponds to a major geodynamic modification, whatever is the origin of this erosion increase (tectonic or climatic, 'chicken or egg' problem, e.g., Molnar and England 1990). We propose that the evolution from a tectonic regime characterized by extrusion and convergent plate conditions to a tectonic regime characterized by gravitational re-equilibration is controlled by a modification in the subtle balance between boundary forces and buoyancy forces. This transition probably took place during Pliocene times, in relation to the decrease of the plate convergence rate, and with the increase of erosion.

Conclusions

We applied a multidisciplinary approach to the analysis of neotectonic deformation around the bend of the Western and Central Alps, including seismotectonics, numerical modeling, GPS, morphotectonics, field work, and brittle deformation analysis. Our 10-year-long researches showed that late Alpine tectonics, from the Neogene onward was characterized by two distinct extensional processes. The first one is interpreted in terms of lateral extrusion of the inner Western Alpine Arc, coeval with Adria indentation, and with the propagation of the thrust front toward the most external parts of the belt. The development of this extensional phase is primarily due to the Adriatic indentation, and second to the opening of the Ligurian Sea. During the Pliocene, a modification in Alpine geodynamics, related to a decrease or a stop of the collision,

and probably to a significant increase in erosion rates in the Alps, led to the development of a second extensional phase, due to body forces in the root of the belt and gravitational re-equilibration. We also characterized the overall seismotectonics of the belt, both in terms of active structures and in terms of stress/strain patterns. The major role of inherited crustal structures has been pointed out, and the synergy between the seismological approach and field observations has allowed to recognizing and characterizing active faults in the Western Alps. Our results also raise several issues, mainly concerning the deep geodynamics of the belt. New data, particularly concerning numerical modeling and the 3D-imagery of lithospheric structures would allow to better constrain these issues: the Alps are still a mysterious and emblematic mountain chain.

References

Ahorner Z, Murawski H, Schneider G (1972) Seismotektonische Traverse von der Nordsee bis zum Apennin. Geol Rundsch 61:915–942

Amitrano D, Grasso JR, Hantz D (1999) From diffuse to localized damage through elastic interaction. Geophys Res Lett 26:2109–2112

Anderson H, Jackson J (1987) Active tectonics in the Adriatic region. Geophys J R Astron Soc 91:937–983

Angelier J (1990) Inversion of field data in fault tectonics to obtain the regional stress–a new rapid direct inversion method by analytical means. Geophys J Int 103:363–376

Augliera P, Cattaneo M, Eva C (1995) Seimic multiplets analysis and its implication in seismotectonics. Tectonophysics 248:219–234

Baroux E, Béthoux N, Bellier O (2001) Analyses of the stress field in southeastern France from earthquake focal mechanisms. Geophys J Int 145:336–348

Bayer R, Carozzo MT, Lanza R, Miletto M, Rey D (1989) Gravity modelling along the ECORS-CROP vertical seimic reflection profile through the Western Alps. Tectonophysics 162:203–218

Béthoux N, Fréchet J, Guyoton F, Thouvenot F, Cattaneo M, Eva C, Nicolas M, Granet M (1992) A closing Ligurian Sea? Pure Appl Geophys 139:179–194

Bigot-Cormier F, Poupeau G, Sosson M (2000) Dénudations différentielles du Massif Cristallin Externe alpin de l'Argentera (Sud-Est de la France) révélées par thermochronologie traces de fission (apatites, zircons). C R Acad SciParis 330:363–370

Bird P (1999) Thin-plate and thin-shell finite-element programs for forward dynamic modeling of plate deformation and faulting. Comput Geosci 25:383–394

Bistacchi A, Dal Piaz GV, Massironi M, Zattin M, Balestrieri ML (2001) The Aosta-Ranzola extensional fault system and Oligo-cene-Present evolution of the Austroalpine-Penninic wedge in the northwestern Alps. Int J Earth Sci 90:654–667

Bogdanoff S, Michard A, Mansour M, Poupeau G (2000) Apatite fission track analysis in the Argentera massif: evidence of contrasting denudation rates in the External Crystalline Massifs of the Western Alps. Terra Nova 12:117–125

Burbank DW, Anderson RS (2001) Tectonic geomorphology. Black-well, Oxford, pp 1–274

Burg JP, Sokoutis D, Bonini M (2002) Model-inspired interpretation of seismic structures in the Central Alps:crustal wedging and buckling at mature stage of collision. Geology 30:643–646

Burkhard M (1988) L'helvétique de la bordure occidentale du massif de l'Aar (évolution tectonique et métamorphique). Eclogae Geol Helvet 81:63–114

Burov E, Podladchikov Y, Grandjean G, Burg JP (1999) Thermo-mechanical approach to validation of deep crustal and litho-spheric structures inferred from multidisciplinary data: applica-tion to the Western and Northern Alps. Terra Nova 11:124–131

Byerlee JD (1978) Frictional characteristics of granite under high pressure. J Geophys Res 72:3639–3648

Calais E, Nocquet JM, Jouanne F, Tardy M (2002) Current strain regime in the Western Alps from continuous Global Positioning System measurements, 1996–2001. Geology 30:651–654

Cannic S, Mugnier JL, Lardeaux JM (1999) Neogene extension in the Western Alps. Mem Sci Geol (Padova) 51:33–45

Carminati E, Wortel MJR, Meijer PT, Sabadini R (1998) The two-stage opening of the western-central Mediterranean basins: a forward modeling to test a new evolutionary model. Earth Planet Sci Lett 160:667–679

Cattin R, Avouac JP (2000) Modeling mountain building and the seismic cycle in the Himalaya of Nepal. J Geophys Res 105:13389–13407

Cederbom CE, Sinclair HD, Schlunegger F, Rahn MK (2004) Climate-induced rebound and exhumation of European Alps. Geology 32:709–712

Champagnac JD, Sue C, Delacou B, Burkhard M (2003) Brittle orogen-parallel extension in the internal zones of the Swiss Alps (south Valais). Eclogae Geol Helvet 96:325–338

Champagnac JD, Sue C, Delacou B, Burkhard M (2004) Brittle deformation in the inner northwestern Alps: from early orogen-parallel extrusion to late orogen-perpendicular collapse. Terra Nova 16:232–242

Champagnac JD, Sue C, Delacou B, Tricart P, Allanic C, Burkhard M (2006) Miocene orogen-parallel extension in the inner Western Alps revealed by dynamical fault analyses. Tectonics. doi: 10.1029/2004TC001779

Champagnac JD, Anderson R, Delacou B, Molnar P, Sue C (2007) Pliocene isostatic rebound of the Western Alps inferred from topographic analysis and sediment budget. Geology. 35(3):195–198. doi:10.1130/G23053

Chéry J, Daignières M, Vilotte JP (1990) How to build an asymmetric crustal root such as the Pyrenean one: a thermomechanical model. Bull Soc Géol France 8(2):211–218

Claudel M, Dumont T, Tricart P (1997) Une preuve d'extension contemporaine de l'expansion océanique de la Téthys ligure en Briançonnais: les failles du Vallon Laugier. C R Acad Sci Paris 325:273–279

Cloetingh S, Burov EB (1996) Thermomechanical structure of European continental lithosphere: constraints from rheological profiles and EET estimates. Geophys J Int 124:695–723

Collombet M, Thomas JC, Chauvin A, Tricart P, Bouillin JP, Gratier JP (2002) Counterclockwise rotation of the Western Alps since the Oligocene: new insights from paleomagnetic data. Tectonics 21:352–366

Coward M, Dietrich D (1989) Alpine tectonics: an overview. In: Coward M, Dietrich D, Park R (eds) Alpine tectonics. Geol Soc London Spec Publ 45:1–29

Dal Piaz GV (1999). Austroalpine-Piedmont nappe stack and the puzzle of Alpine Tethys. In: Gosso G, Jadoul F, Sella F, Spalla MI (eds) Third workshop on alpine geological studies, Padova. Mem Sci Geol 51:155–176

Deichmann N, Garcia-Fernandez M (1992) Rupture geometry from high-precision relative hypocenter locations of microearthquakes clusters. Geophys J Int 110:501–517

Delacou B, Sue C, Champagnac JD, Burkhard M (2004) Present-day geodynamics in the bend of the Western and Central Alps as constrained by earthquake analysis. Geophys J Int 158:753–774

Delacou B, Sue C, Champagnac JD, Burkhard M (2005a) Origin of the current stress field in the Western/Central Alps: role of gravitational reequilibration constrained by numerical model-ling. Geol Soc London Spec Publ 243:295–310

Delacou B, Deichmann N, Thouvenot F, Sue C, Champagnac JD, Burkhard M (2005b) Active strike-slip faulting in the Chablais area (NW Alps) from earthquake focal mechanisms and relative locations. Eclogae Geol Helvet 98:189–199

Dewey JF, Hempton MR, Kidd WSF, Saroglu F, Sengör AMC (1986) Shortening of continental lithosphere: the neotectonics of eastern Anatolia–a young collision zone. In: Coward MP, Ries AC (eds) Collision tectonics. Geol Soc London Spec Publ 19:3–36

England P, Houseman G (1989) Extension during active convergence, with application to the Tibetan Plateau. J Geophys Res 94:17561–17579

Eva E, Solarino S (1998) Variations of stress directions in the Western Alpine arc. Geophys J Int 135:438–448

Eva E, Pastore S, Deichmann N (1998) Evidence for ongoing extensional deformation in the Western Swiss Alps and thrust-faulting in the Southwestern Alpine foreland. J Geodynamics 26:27–43

Fäh D, Giardini D, Bay F, Bernardi F, Braunmiller J, Deichmann N, Furrer M, Gantner L, Gisler M, Isenegger D, Jimenez MJ, Kästly P, Koglin R, Masciadri V, Rutz M, Scheidegger C, Schibler R, Schorlemmer D, Schwarz-Zanetti S, Steimen S, Sellami S, Wiemer S, Wössner J (2003) ECOS and the related macrose-ismic database. Eclogae Geol Helvet 96:219–236

Fleitout L, Froidevaux C (1982) Tectonics and topography for lithosphere containing density heterogeneities. Tectonics 1:21–56

Foeken JPT, Dunai TJ, Bertotti G, Andriessen PAM (2003) Late Miocene to present exhumation in the Ligurian Alps (Southwest Alps) with evidence for accelerated denudation during the Messinian salinity crisis. Geology 31:797–800

Fréchet J (1978) Sismicité du sud-est de la France et une nouvelle méthode de zonage sismique. Thèse de 3ème cycle, Grenoble pp 1–178

Fréchet J (1985) Sismogénèse et doublets sismiques. Thèse d'état Grenoble, France pp 1–324

Frey M, Desmons J, Neubauer F (1999) Metamorphic maps of the Alps. Schweiz Mineral Petrogr Mitt 79:1–4

Giardini D, Grünthal G, Shedlock K, Zhang P (1999) The GSHAP Global Seismic Hazard Map. Ann Geofisica 42:1225–1230

Gidon M (1974) L'arc alpin a-t-il une origine tourbillonnaire ? C R Acad Sci Paris 278:21–24

Grosjean G, Sue C, Burkhard M (2004) Late Neogene brittle extension in the vicinity of the Simplon fault zone, Central Alps, Switzerland. Eclogae Geol Helvet 97:33–46

Gubler E, Kahle HG, Klingele E, Mueller S, Olivier R (1981) Recent crustal movements in Switzerland and their geophysical interpretation. Tectonophysics 71:125–152

Gudmundsson GH (1994) An order-of-magnitude estimate of the current uplift-rates in Switzerland by the Würm Alpine deglaciation. Eclogae Geol Helvet 87:545–557

Guéguen Y, Palciauskas V (1992) Introduction à la physique des roches. Hermann, Paris pp 1–299

Gueguen E, Doglioni C, Fernandez M (1998) On the post-25 Ma geodynamic evolution of the Western Mediterranean. Tectonophysics 298:259–269

Hassani R, Chéry J (1996) Anelasticity explains topography associated with Basin and Range normal faulting. Geology 24:1095–1098

Hassani R, Jongmans D, Chéry J (1997) Study of plate deformation and stress in subduction processes using two-dimensional numerical models. J Geophys Res 102:17951–17965

Hu JC, Angelier J (2004) Stress permutations: three dimensional distinct element analysis account for a common phenomenon in brittle tectonics. J Geophys Res 109. doi:10.1029/2003JB002616

Hubbard M, Mancktelow NS (1992) Lateral displacement during Neogene convergence in the Western and Central Alps. Geology 20:943–946

Ivy-Ochs S, Schäfer J, Kubik PW, Synal HA, Schlüchter C (2004) Timing of deglaciation on the Northern Alpine foreland (Switzerland). Eclogae Geol Helvet 97:47–55

Jackson J, McKenzie D (1988) The relationship between plate motion and seismic moment tensors, and the rates of active deformation in the Mediterranean and Middle East. Geophys J R Astr Soc 93:45–73

Jolivet L, Goffé B, Bousquet R, Oberhänsli R, Michard A (1998) Detachments in high-pressure mountain belts, Tethyan examples. Earth Planet Sci Lett 160:31–47

Kahle HG, Geiger A, Buerki B, Gubler E, Marti U, Wirth B, Rothacher M, Gurtner W, Beutler G, Bauersima I, Pfiffner OA (1997) Recent crustal movements, geoid and density distribution; contribution from integrated satellite and terrestrial measurements. In: Pfiffner OA, Lehner P, Heitzmann P, Mueller S, Steck A (eds) Deep structure of the Swiss Alps: results of NRP20. Birkhäuser Verlag, Basel, pp 251–259

Kastens K, Mascle J (1990) The geological evolution of the Tyrrhenian sea: an introduction to scientific results of ODP leg 107. Proc ODP Sci Results 107:3–26

Kastrup U, Zoback ML, Deichmann N, Evans K, Giardini D (2004) Stress field variations in the Swiss Alps and the Northern Alpine foreland derived from inversion of fault plane solutions. J Geophys Res 109 doi:10.1029/2003JB002550

Kelly MA, Buoncristiani JF, Schlüchter C (2004) LGM ice-surface reconstruction, Western Swiss Alps. Eclogae Geol Helvet 97:57–77

Kirby SH, Kronenberg AK (1987) Rheology of the lithosphere. Rev Geophys 25:1219–1244

Klemann V, Wolf D (1998) Modelling of stresses in the Fennoscandian lithosphere induced by Pleistocene glaciations. Tectonophysics 294:291–303

Kong X, Bird P (1995) SHELLS: a thin-shell program for modeling neotectonics of regional or global lithosphere with faults. J Geophys Res 100:22129–22131

Kuhlemann J, Kempf O (2002) Post-Eocene evolution of the North Alpine Foreland Basin and its response to Alpine tectonics. Sediment Geol 152:45–78

Kuhlemann J, Frisch W, Szekely B, Dunkl I, Kazmer M (2000) Post-collisional sediment budget history of the Alps: tectonic versus climatic control. Int J Earth Sci 91:818–837

Kuhlemann J, Frisch W, Szekely B, Dunk I, Kazmer M (2002) Post-collisional sediment budget history of the Alps: tectonic versus

climatic control. Int J Earth Sci 91:818–837. doi:10.1007/s00531-002-0266-y

Lacassin R, Tapponnier P, Meyer B, Armijo R (2001) Was the Trévaresse thrust the source of the 1909 Lambesc (Provence, France) earthquake? Historical and geomorphic evidence. Earth Planet Sci Lett 333:571–581

Lacombe O, Mouthereau F (2002). Basement-involved shortening and deep detachment tectonics in forelands of orogens; insights from recent collisions belts; Taiwan, Western Alps, Pyrenees. Tectonics 21 doi:10.1029/2001TC901018

Laubscher H (1991) The arc of the Western Alps today. Eclogae Geol Helvet 84:631–659

Le Pichon X, Chamot-Rooke N, Lallemant SL, Noomen R, Veis G (1994) Geodetic determination of the kinematics of Central Greece with respect to Europe: implication for the Eastern Mediterranean tectonics. J Geophys Res 100:12675–12690

Lemoine M, Bas T, Arnaud-Vanneau A, Arnaud A, Dumont T, Gidon M, Bourbon M, de Graciansky PC, Rudkiewicz JL, Mégard-Galli J, Tricart P (1986) The continental margin of the Mesozoic Tethys in the Western Alps. Mar Petrol Geol 3:179–199

Lickorish WH, Ford M, Bürgisser J, Cobbold PR (2002) Arcuate thrust systems in sandbox experiments: a comparison to the external arcs of the Western Alps. Geol Soc Am Bull 114:1089–1107

Lippitsch R, Kissling E, Ansorge J (2003) Upper mantle structure beneath the Alpine orogen from high-resolution teleseismic tomography. J Geophys Res 108 doi:10.1029/2002JB002016

Malusa MG, Polino R, Zattin M, Bigazzi G, Martin S, Piana F (2005) Miocene to present differential exhumation in the Western Alps: insights from fission track thermochronology. Tectonics 24:1–23

Marchant RH, Stampfli GM (1997) Crustal and lithospheric structure of the Western Alps: geodynamic significance. In: Pfiffner OA, Lehner P, Heitzmann P, Mueller S, Steck A (eds) Deep structure of the Swiss Alps: results of NRP20. Birkhäuser Verlag, Basel, pp 326–337

Marrett R, Peacock DCP (1999) Strain and stress. J Struct Geol 21:1057–1063

Martinod J, Jouanne F, Taverna J, Ménard G, Gamond JF, Darmendrail X, Notter JC, Basile C (1996) Present-day deformation of the Dauphiné (SE France) Alpine and Subalpine massifs. Geophys J Int 127:189–200

Martinod J, Roux L, Gamond JF, Glot JP (2001) Present-day deformation of the Belledonne Massif (External Alps, France): comparison triangulation-GPS. Bull Soc Géol France 172:713–721

Masson F, Verdun J, Bayer R, Debeglia N (1999) A new gravity map of the western Alps and its structural and tectonic consequences: une nouvelle carte gravimetrique des Alpes occidentales et ses consequences structurales et tectoniques. C R Acad Sci Paris 329:865–871

Maurer H, Deichmann N (1995) Microearthquake cluster detection based on waveform similarities, with an application to the Western Swiss Alps. Geophys J Int 123:588–600

Maurer H, Burkhard M, Deichmann N, Green AG (1997) Active tectonism in the Central Alps: contrasting stress regimes north and south of the Rhone Valley. Terra Nova 9:91–94

Ménard G (1979) Relations entre structures profondes et structures superficielles dans le Sud-Est de la France; essai d'utilisation de données géophysiques. PhD thesis, Grenoble pp 1–178

Ménard G (1988) Structure et cinématique d'une chaîne de collision: Les Alpes occidentales et centrales. Thèse de Doctorat d'état. Grenoble pp 1–278

Ménard G, Molnar P (1988) Collapse of the Hercynian Tibetan Plateau into a late Paleozoic European Basin and Range Province. Nature 334:235–237

Molnar P, England P (1990) Late Cenozoic uplift of mountain ranges and global climate change: chicken or egg? Nature 346:29–34

Molnar P, Lyon-Caen H (1988) Some simple physical aspects of the support, structure, and evolution of mountain belts. Geol Soc Am Bull 218:179–207

Molnar P, Tapponnier P (1975) Cenozoic tectonics of Asia: effect of a continental collision. Science 189:419–425

Molnar P, England P, Martinod J (1993) Mantle dynamics, the uplift of the Tibetan plateau and the Indian monssoon. Rev Geophys 31:123–153

Nicolas A, Hirn A, Nicolich R, Polino R, Group ECW (1990) Lithospheric wedging in the Western Alps inferred from the ECORS-CROP traverse. Geology 18:587–590

Nocquet JM, Calais E (2003) Crustal velocity field of Western Europe from permanent GPS array solutions, 1996–2001. Geophys J Int 154:72–88

Nocquet JM, Calais E (2004) Geodetic measurements of crustal deformation in the Western Mediterranean and Europe. Pure Appl Geophys 161:661–681

Paul A, Cattaneo M, Thouvenot F, Spallarossa D, Béthoux N, Fréchet J (2001) A three-dimensional crustal structure velocity model of the South-western Alps from local earthquake tomography. J Geophys Res 106:19367–19389

Pavoni N (1980a) Comparison of focal mechanisms of earthquakes and faulting in the Helvetic zone of the Central Valais, Swiss Alps. Eclogae Geol Helvet 73:551–558

Pavoni N (1980b) Crustal stresses inferred from fault-plane solutions of earthquakes and neotectonic deformation in Switzerland. Rock Mech Suppl 9:63–68

Persaud M, Pfiffner OA (2004) Active deformation in the Eastern Swiss Alps: post-glacial faults, seismicity and surface uplift. Tectonophysics 385:59–84

Polino R, Dal Piaz G, Gosso G (1990). Tectonic erosion at the Adria margin and accretionary processes for the Cretaceous orogeny of the Alps. In: Roure F, Heitzmann P, Polino R (eds) Deep structure of the Alps. Mém Soc Géol France 157:345–367

Ratschbacher L, Frisch W, Neubauer F, Schmid SM, Neugebauer J (1989) Extension in compressional orogenic belts : the Eastern Alps. Geology 17:404–407

Rolland Y, Lardeaux JM, Guillot S, Nicollet C (2000) Extension syn-convergence, poinçonnement vertical et unites métamorphiques contrastées en bordure ouest du Grand Paradis (Alpes Franco-Italiennes). Geodinamica Acta 13:133–148

Rollet N, Deverchere J, Beslier MO, Guennoc P, Rehault JP, Sosson M, Truffert C (2002) Back arc extension, tectonic inheritance, and volcanism in the Ligurian Sea, Western Mediterranean. Tectonics 21:218–243

Rosenbaum G, Lister GS (2004a) Neogene and Quaternary rollback evolution of the Tyrrhenian Sea, the Apennines, and the Sicilian Maghrebides. Tectonics 23 doi:10.1029/2003TC001518

Rosenbaum G, Lister GS (2004b) Formation of arcuate orogenic belts in the Western Mediteranean region. Geol Soc Am Bull 383:41–56

Rothé JP (1941) Les séismes des Alpes françaises en 1938 et la sismicité des Alpes occidentales. Ann Inst Phys Globe Strasb 3:1–105

Roure F, Bergerat F, Damotte B, Mugnier JL, Polino R (1996) The ECORS-CROP Alpine seismic traverse. In Roure F, Heitzmann P, Polino R (eds). Deep structure of the Alps. Mém Soc Géol France 157:367–379

Schaer JP, Jeanrichard F (1974) Mouvements verticaux anciens et actuels dans les Alpes suisses. Eclogae Geol Helvet 67:101–119

Schmid SM, Kissling E (2000) The arc of the Western Alps in the light of geophysical data on deep crustal structure. Tectonics 19:62–85

Schmid S, Zingg A, Handy M (1987) The kinematics of movement along the Insubric Line and emplacement of the Ivrea Zone. Tectonophysics 135:47–66

Schmid S, Fügenschuh B, Kissling E, Schuster R (2004) Tectonic map and overall architecture of the Alpine orogen. Eclogae Geol Helvet 97:93–117

Scholtz CH (1990) The mechanics of earthquakes and faulting. Cambridge University Press, Cambridge, pp 1–369

Scholtz CH (1998) Earthquakes and friction laws. Nature 391:37–42

Selverstone J (2005) Are the Alps collapsing? Annu Rev Earth Planet Sci 33:113–132

Seward D, Mancktelow NS (1994) Neogene kinematics of the Central and Western Alps: evidence from fission-track dating. Geology 22:803–806

Seyferth M, Henk A (2004) Syn-convergent exhumation and lateral extrusion in continental collision zones–insights from three-dimensional numerical models. Tectonophysics 382:1–29

Sibson RH (2003) Thickness of the seismic slip zone. Bull Seism Soc Am 93:1169–1178

Sommaruga A (1999) Decollement tectonics in the Jura foreland fold-and-thrust belt. Mar Petrol Geol 16:111–134

Spakman W, Wortel R (2004) A tomographic view on the Western Mediterranean geodynamics, In: Cavazza RF, Spakman W, Stampfli GM, Ziegler PA (eds) The TRANSMED Atlas—the Mediterranean region from crust to mantle. Springer, Berlin Heidelberg New York, pp 31–52

Stampfli G (1993) Le Briançonnais, terrain exotique dans les Alpes? Eclogae Geol Helvet 1:1–45

Stampfli G, Mosar J, Marquer D, Marchant R, Baudin T, Borel G (1998) Subduction and obduction processes in the Swiss Alps. Tectonophysics 296:159–204

Steck A, Hunziker J (1994) The Tertiary structure and thermal evolution of the Central Alps–compressional and extensional structures in an orogenic belt. Tectonophysics 238:229–254

Sue C, Tricart P (1999) Late Alpine brittle extension above the Frontal Pennine Thrust near Briançon, Western Alps. Eclogae Geol Helvet 92:171–181

Sue C, Tricart P (2002) Widespread post-nappe normal faulting in the internal Western Alps: a new constrain on arc dynamic. J Geol Soc London 159:61–70

Sue C, Tricart P (2003) Neogene to ongoing normal faulting in the inner Western Alps: a major evolution of the late alpine tectonics. Tectonics 22:1–25

Sue C, Thouvenot F, Fréchet J, Tricart P (1999) Widespread extension in the core of the Western Alps revealed by earthquake analysis. J Geophys Res 104:25611–25622

Sue C, Martinod J, Tricart P, Thouvenot F, Gamond JF, Frechét J, Marinier D, Glot JP, Grasso JR (2000) Active deformation in the inner Western Alps inferred from comparison between 1972-classical and 1996-GPS geodetic surveys. Tectonophysics 320:17–29

Sue C, Grasso JR, Lahaie F, Amitrano D (2002) Mechanical behavior of western alpine structures inferred from statistical analysis of seismicity. Geophys Res Lett 29:65–69

Sue C, Delacou B, Burkhard M, Champagnac JD, Allanic C (2007) Seismic strain of the Western Alps. Terra Nova. doi:10.1111/j.1365-3121.2007.00732.x

Tapponnier P (1977) Evolution tectonique du système alpin en Méditerranée: Poinçonnement et écrasement rigide-plastique. Bull Soc Géol France 7:437–460

Thouvenot F, Fréchet J, Tapponnier P, Thomas JC, Le Brun B, Ménard G, Lacassin R, Jenatton L, Grasso JR, Coutant O, Paul A, Hatzfeld D (1998) The Ml 5.3 Epagny (French Alps) earthquake of 1996 July 15: a long-awaited event on the Vuache Fault. Geophys J Int 135:876–892

Thouvenot F, Fréchet J, Jenatton L, Gamond JF (2003) The belledonne border fault: identification of active seismic strike-slip fault in the Western Alps. Geophys J Int 155:174–192

Tricart P (1984) From passive margin to continental collision: a tectonic scenario for the Western Alps. Am J Sci 284:97–120

Van der Beek PA, Braun J (1999) Controls on post-mid-Cretaceous landscape evolution in the Southeastern Highlands of Australia: insights from numerical surface process models. J Geophys Res 104:4945–4966

Vialon P, Rochette P, Ménard G (1989) Indentation and rotation in the Alpine arc. In: Coward M, Dietrich D, Park R (eds) Alpine tectonics. Geol Soc London Spec Publ 45:329–338

Von Blanckenburg F, Davies JH (1995) Slab breakoff: a model for syncollisional magmatism and tectonics in the Alps. Tectonics 14:120–131

Waldhauser F, Kissling E, Ansorge J, Mueller S (1998) Three-dimensional interface modelling with two-dimensional seimic data: the alpine crust-mantle boundary. Geophys J Int 135:264–278

Wawrzyniec TF, Selverstone J, Axen GJ (2001) Style of footwall uplift along the simplon and brenner normal fault system, Central and Eastern Alps. Tectonics 20:748–770

Wessel P, Smith WH (1991) Free software helps map and display data. EOS Trans Am Geophys Union 72:441 and 445–446

Whipple KX, Kirby E, Brocklehurst SH (1999) Geomorphic limits to climate-induced increases in topographic relief. Nature 401:39–43

Wortmann UG, Weissert H, Funk H, Hauck J (2001) Alpine plate kinematics revisited: the adria problem. Tectonics 20:134–147

Wu P, Johnston P, Lambeck K (1999) Postglacial rebound and fault instability in Fennoscandia. Geophys J Int 139:657–670

Zhang J, Lin D, Dalai Z, Yong Z (2000) Orogen-parallel extension in Himalaya: is it the indicator of collapse or the product in process of compressive uplift? Chin Sci Bull 45:114–119